Monthly Notices of the ROYAL ASTRONOMICAL SOCIETY
MNRAS **454,** 2120–2145 (2015) doi:10.1093/mnras/stv2075

Galaxy and mass assembly (GAMA): projected galaxy clustering

D. J. Farrow,[1,2⋆] Shaun Cole,[1⋆] Peder Norberg,[1,3⋆] N. Metcalfe,[3] I. Baldry,[4] Joss Bland-Hawthorn,[5] Michael J. I. Brown,[6] A. M. Hopkins,[7] Cedric G. Lacey,[1] J. Liske,[8] Jon Loveday,[9] David P. Palamara,[6] A. S. G. Robotham[10] and Srivatsan Sridhar[9†]

[1]*ICC, Department of Physics, University of Durham, South Road, Durham DH1 3LE, UK*
[2]*Max-Planck-Institut für extraterrestrische Physik, Postfach 1312 Giessenbachstrasse, D-85741 Garching, Germany*
[3]*CEA, Department of Physics, University of Durham, South Road, Durham DH1 3LE, UK*
[4]*Astrophysics Research Institute, Liverpool John Moores University, IC2, Liverpool Science Park, 146 Brownlow Hill, Liverpool L3 5RF, UK*
[5]*Sydney Institute for Astronomy, School of Physics A28, University of Sydney, NSW 2006, Australia*
[6]*School of Physics and Astronomy, Monash University, Clayton, Victoria 3800, Australia*
[7]*Australian Astronomical Observatory, PO Box 915, North Ryde, NSW 1670, Australia*
[8]*Hamburger Sternwarte, Universität Hamburg, Gojenbergsweg 112, D-21029 Hamburg, Germany*
[9]*Astronomy Centre, University of Sussex, Falmer, Brighton BN1 9QH, UK*
[10]*ICRAR M468, University of Western Australia, 35 Stirling Hwy, Crawley, WA 6009, Australia*

Accepted 2015 September 4. Received 2015 September 4; in original form 2015 May 29

ABSTRACT

We measure the projected two-point correlation function of galaxies in the 180 deg^2 equatorial regions of the GAMA II survey, for four different redshift slices between $z = 0.0$ and 0.5. To do this, we further develop the Cole method of producing suitable random catalogues for the calculation of correlation functions. We find that more r-band luminous, more massive and redder galaxies are more clustered. We also find that red galaxies have stronger clustering on scales less than $\sim 3\,h^{-1}$ Mpc. We compare to two different versions of the GALFORM galaxy formation model, Lacey et al. (in preparation) and Gonzalez-Perez et al., and find that the models reproduce the trend of stronger clustering for more massive galaxies. However, the models underpredict the clustering of blue galaxies, can incorrectly predict the correlation function on small scales and underpredict the clustering in our sample of galaxies with $\sim 3L_r^*$. We suggest possible avenues to explore to improve these clustering predictions. The measurements presented in this paper can be used to test other galaxy formation models, and we make the measurements available online to facilitate this.

Key words: galaxies: evolution – galaxies: formation – large-scale structure of Universe.

1 INTRODUCTION

The two-point autocorrelation function is a widely used statistical description of the spatial distribution of galaxies. In the standard model of cosmology, the shape of this function is set both by the mass of dark matter haloes in which a particular galaxy sample resides, and baryonic processes which can change the spatial distribution of galaxies on smaller scales. Its dependence on galaxy properties is well established, at low redshifts, by large-area spectroscopic surveys such as SDSS (York et al. 2000; Strauss et al. 2002) and Two Degree Field Galaxy Redshift Survey (2dFGRS; Colless et al. 2001). The amplitude of the autocorrelation function of galaxies is seen to be strongly dependent on luminosity, stellar mass and colour. At low redshifts, brighter, redder and more massive galaxies have been observed to be more strongly clustered (e.g. Norberg et al. 2001, 2002; Zehavi et al. 2002, 2005, 2011; Li et al. 2006; Christodoulou et al. 2012).

In the higher redshift Universe, small (<1 deg^2) but deep spectroscopic surveys have also measured the clustering of galaxies. The DEEP2 survey has been used to demonstrate that the colour dependence of galaxy clustering is already in place at $z \sim 1$, whilst within a red or blue sample of galaxies, clustering is insensitive to luminosity over the range $20.2 < M_B < 21.8$ (Coil et al. 2008). Compared with lower redshift SDSS data, the DEEP2 measurements of the clustering of brighter and more massive galaxies has a larger amplitude than expected from scaling the low-redshift measurements using linear theory (Coil et al. 2008; Li et al. 2012). This can be interpreted as evidence of significant bias evolution for these galaxies (Coil et al. 2008; Li et al. 2012). Another example of

⋆E-mail: dfarrow@mpe.mpg.de (DJF); shaun.cole@durham.ac.uk (SC); peder.norberg@durham.ac.uk (PN)
† Present address: Laboratoire J. L. Lagrange, Observatoire de la Côte d'Azur, BP4429, 06300, Nice, France.

a small area, deep spectroscopic survey is the VIMOS-VLT Deep Survey (VVDS), which found a sharp increase in the amplitude of galaxy clustering around the characteristic magnitude of the sample's luminosity function (Pollo et al. 2006). VVDS also found, in agreement with DEEP2, that the clustering of massive galaxies, with stellar mass $>10^{10.5}\,h^{-2}\,\mathrm{M}_{\odot}$, at $z\sim1$ can only be reconciled with lower redshift measurements if their bias evolves significantly (Meneux et al. 2008). Results from another small area, deep survey, zCOSMOS, show that this is true for galaxies more massive than $>10^{10}\,h^{-2}\,\mathrm{M}_{\odot}$ (Meneux et al. 2009). The VIMOS Public Extragalactic Redshift Survey (VIPERS) has also found that more luminous and more massive galaxies are more clustered at redshifts of $0.5<z<1.1$ than their fainter, less massive counterparts (de la Torre et al. 2013; Marulli et al. 2013). More recently, the 9 deg^2 PRIMUS survey (Coil et al. 2011; Cool et al. 2013) has found red galaxies that are more clustered than blue galaxies, and the relationship between clustering amplitude and sample luminosity is in place in the redshift slices: $0.2<z<0.5$ and $0.5<z<1.0$ (Skibba et al. 2014).

In addition to spectroscopic surveys, surveys relying on photometric redshifts have also explored the clustering of galaxies. Galaxies with red colours have been shown to have steeper correlation functions than bluer galaxies at $z\sim0.5$ in the 0.78 deg^2 COMBO-17 survey (Phleps et al. 2006), and the 1.5 deg^2 Ultra-VISTA survey demonstrated that more massive galaxies are more clustered between $0.5<z<2.5$ (McCracken et al. 2015). Photometric surveys have also studied the evolution of galaxy clustering. In the 6.96 deg^2 Boötes field Brown et al. (2008) found, at $0.2<z<1.0$, that red galaxies fainter than $M_B=20-5\log_{10}h$ showed no luminosity dependence of the amplitude of their clustering, whilst the converse is true for red galaxies brighter than this. Studies in the Boötes field also demonstrated luminous red galaxies display little evolution in the amplitude of their clustering between $z=0.5$ and 0.9 (White et al. 2007; Brown et al. 2008). This observation, which suggests the clustering of these galaxies evolves slower than the underlying dark matter distribution, can be explained by the removal of highly biased satellite galaxies by merging or disruption (White et al. 2007; Brown et al. 2008). Whilst bright, red galaxies display little evolution in clustering strength with redshift, fainter galaxies ($-22<M_B-5\log_h<-19$) have been shown to have a decreasing clustering amplitude between $z=0.4$ and 1.2 in the CFHTLS photometric redshift survey (McCracken et al. 2008).

The photometric surveys at high redshift are still fairly small (<10 deg.^{2}). A possible exception to the trade-off between large area and high redshift is the work of Guo et al. (2014); here, the authors used the CMASS sample of SDSS to show that clustering was stronger for brighter and redder galaxies at $z\sim0.5$. However, the complicated selection of the CMASS sample limits their work to a very narrow luminosity and redshift range.

The GAMA spectroscopic survey offers a new window on to the clustering of galaxies and its evolution with redshift. It has a larger area (the equatorial regions we use total 180 deg^2) than the deep surveys but has spectra of much fainter galaxies (2 mag) than large-area surveys like SDSS. As such, it complements both types of survey, by enabling detailed clustering measurements at an intermediate epoch. Whilst our redshift range overlaps with the PRIMUS low-redshift sample, our larger area allows us to split the data into finer redshift bins and consider brighter, rarer objects. In this paper, we study the projected two-point correlation function (2PCF) of galaxies as a function of their luminosity, stellar mass and colour, in four different redshift bins, in order to fully appreciate any redshift evolution. To aid in the physical interpretation of our results, we compare them to different versions of the semi-analytic galaxy formation model GALFORM, specifically Gonzalez-Perez et al. (2014, hereafter G14 model) and Lacey et al. (in preparation, hereafter L14 model). We quantitatively compare the relative merits of the different versions of the GALFORM model and discuss the impact of this on our understanding of galaxy formation. To see a complementary approach, we refer the reader to Palamara et al. (in preparation), who fit halo occupation distribution models (HOD models; see e.g. Zheng et al. 2005) to GAMA.

This paper is organized as follows. Section 2 introduces the GAMA data and the galaxy formation model we use, along with details of how we calculate luminosity, mass and rest-frame colour. Section 3 presents our method of generating a random catalogue and measuring clustering. In Section 4 we present our results, before discussing them and concluding in Section 5. We present our results using units of a fiducial Λ cold dark matter (ΛCDM) cosmology with $\Omega_\mathrm{m}=0.25$, $\Omega_\Lambda=0.75$ and $H=100\,h$ km s^{-1} Mpc^{-1}.

2 DATA AND MODELS

2.1 The galaxy and mass assembly survey

The GAMA survey is a spectroscopic and multiwavelength survey of galaxies carried out on the Anglo-Australian telescope (Driver et al. 2011; Liske et al. 2015). In this work, we utilize the main r-band limited data from the GAMA II equatorial regions, which consists of a highly complete (>98 per cent) spectral catalogue of galaxies selected from the SDSS DR7 (Abazajian et al. 2009) to have $r_\mathrm{petro}<19.8$. The older GAMA I survey had a shallower limit of $r<19.4$ in two of the regions. Target fields are repeatedly observed in a way that removes biases against close pairs (Robotham et al. 2010), avoiding such biases is ideal for clustering measurements. Star/galaxy separation is based on the difference between an object's model and point spread function magnitudes in SDSS DR7 data and, where UKIRT Infrared Deep Sky Survey photometry is available, the object's optical and infrared colours. Further details of the GAMA survey are given in Baldry et al. (2010), Robotham et al. (2010), Driver et al. (2011) and Liske et al. (2015). The data are split over three 12×5 deg^2 fields centred at 9^h (G09), 12^h (G12) and 14.5^h (G15) RA and approximately $\delta=0^\circ$ declination.

2.1.1 *Redshifts*

Redshifts for GAMA objects were measured automatically, using the software AUTOZ as described in Baldry et al. (2014). Liske et al. (2015) find 0.2 per cent of the sample are expected to have an incorrect redshift. The median velocity uncertainty of the measured redshifts is 27 km s^{-1} (Liske et al. 2015). The redshifts are taken from a table called DISTANCESFRAMESV12 in a GAMA Data Management Unit (DMU). These redshifts have been corrected for the local flow using the model of Tonry et al. (2000), smoothly tapered to the cosmic microwave background rest frame for $z\geq0.03$.

2.1.2 *Quality cuts*

In addition to the redshift quality cut, $nQ\geq3$, we also only consider galaxies in regions with completeness greater than 80 per cent using the GAMA angular completeness mask (Driver et al. 2011; Liske et al. 2015). We additionally only select objects with VIS_CLASS = 0, VIS_CLASS = 1 or VIS_CLASS = 255, which removes objects which upon visual inspection do not show any evidence of galaxy light or appear to be part of another galaxy (Baldry et al. 2010).

2.1.3 *Magnitudes*

GAMA combines data from a large number of ground and space based telescopes and so has a very wide wavelength range, from X-ray to radio. In this work, we use optical photometry from SDSS DR7 imaging data. To define luminosity samples we use SDSS Petrosian magnitudes (Petrosian 1976), as the GAMA selection used Petrosian magnitudes. To define colours, and when estimating stellar mass, we use SDSS model magnitudes as these are often more suitable for colour terms (see the SDSS DR7 photometry webpage[1]). Following SDSS conventions, we will label model magnitudes using the letter associated with the bandpass in which the magnitude was measured. We took these magnitudes from the table called TilingCatv42 in a GAMA DMU, where they are replicated.

GAMA also has a set of magnitudes measured in apertures with a matched size across the different bands (Hill et al. 2011), these magnitudes have been shown to be superior to model magnitudes when calculating a galaxy's stellar mass using spectral energy distribution (SED) fitting (Taylor et al. 2011). Our adoption of model magnitudes was in order to avoid the small number of failures whose spatial positions have not been mapped in the Hill et al. (2011) catalogue. Model magnitudes have been widely used to define colours in SDSS publications, and should be sufficient to separate red and blue galaxies in this work.

2.1.4 *k-corrections and evolution corrections*

To compute Petrosian absolute r-band magnitudes, $M_r - 5\log_{10} h$ (hereafter $M_{r,h}$), from the observed apparent Petrosian r-band magnitudes, m_r, we apply both a k-correction, k_r, and a luminosity evolution correction. The latter correction is necessary in order to compare a similar population of galaxies across time, as the luminosity of galaxies evolves. The relation we use is

$$M_{r,h} = m_r - k_r(z) + Q(z - z_{\rm ref}) - 5\log_{10}(D_{\rm L}(z)) - 25, \quad (1)$$

where Q is the luminosity evolution parameter, $D_{\rm L}$ the luminosity distance in h^{-1} Mpc and $z_{\rm ref}$ is a reference redshift, for which we adopt $z_{\rm ref} = 0.0$. The parametrization of luminosity evolution we use is commonly adopted in the literature (e.g. Lin et al. 1999; Loveday et al. 2012).

At this stage, we will also introduce a parametrization of density evolution common to luminosity function studies. The P parameter (e.g. Lin et al. 1999; Loveday et al. 2012, and references therein) parameterizes the density evolution of a population of galaxies via

$$\phi^*(z) = \phi^*(z = 0)10^{0.4Pz}, \quad (2)$$

where $\phi^*(z)$ is the characteristic number density of galaxies at redshift z. Loveday et al. (2012) have fit evolving luminosity functions to a shallower version of the GAMA data, with a limit of $r_{\rm petro} < 19.4$ in G09 and G15. They find that Q and P are very degenerate (see also Farrow 2013). In Loveday et al. (2015) adopting a value of $Q = 1.45$ resulted in very little need for density evolution (see also Farrow 2013). We therefore adopt $Q = 1.45$, which combined with our method of generating a random catalogue, removes the need to correct for density evolution (see Section 3.1). Note that in Loveday et al. (2015), a different set of parameters are favoured. However in Appendix A, we show that adopting the parameters $P = 1.45$ and $Q = 0.81$, which we took from an earlier draft of Loveday et al. (2015), affects the correlation function in a way far smaller than the errors.

The k-corrections are derived from the GAMA DMU kcorr_z00v04, which was produced using the method set out in Loveday et al. (2012). The Loveday et al. (2012) k-corrections are found by using the code kcorrect_v4_2 (Blanton & Roweis 2007) to fit each galaxy's u, g, r, i, and z-band SDSS model magnitudes with SED templates. For many applications, the maximum redshift at which an object fulfils the selection criteria of the survey, $z_{\rm max}$, is needed. For this, the k-correction as a function of redshift is required for each galaxy. To enable fast computation, Loveday et al. (2012) fit a fourth-order polynomial to the k-correction of each galaxy as a function of redshift. The rms difference between the kcorrect estimates of k-correction and the polynomial fits to them is less than 0.01 mag for all bands (Loveday et al. 2012). We further speed up the k-correction process by using average polynomials from McNaught-Roberts et al. (2014), who computed the median of the Loveday et al. (2012) k-correction polynomials for galaxies in seven, $(g - r)$ rest frame colour bins, hereafter labelled $(g - r)_0$. The benefit of this is a reduction in noise introduced by fitting each galaxy with an individual model (McNaught-Roberts et al. 2014). Rest-frame colours are still estimated from the individual k-corrections of Loveday et al. (2012).

2.1.5 *Stellar mass*

As well as luminosity and colour, we also want to use GAMA II to measure clustering as a function of stellar mass. We use the relation between colour and stellar mass found for GAMA I data by Taylor et al. (2011), namely

$$\log_{10} M_*(h^{-2}\,{\rm M}_\odot) = 1.15 + 0.7(g - i)_0 - 0.4(M_i - 5\log_{10} {\rm h}), \quad (3)$$

where M_i is the rest-frame i-band absolute model magnitude and $(g - i)_0$ is the rest-frame colour. This relation was found by Taylor et al. (2011) from individual estimates of the stellar mass of GAMA I galaxies, produced by fitting stellar population synthesis (SPS) models to the optical GAMA data (details in Taylor et al. 2011). These mass estimates should have a statistical 1σ accuracy of around 0.1 dex (Taylor et al. 2011). The original relation used the GAMA matched-aperture magnitudes for the colours, whilst we use SDSS model magnitudes. We have tested that this does not add significant biases or scatter to our computed stellar masses. The resultant offset between our mass-to-light ratios and the ones utilizing the GAMA matched aperture colours with equation (3) is only 0.01 dex with an interquartile range of 0.1 dex and 10 per cent of outliers with a difference of >0.14 dex. Note that the problem Taylor et al. (2011) discovered with masses using model magnitudes arose during full SED fitting, not using this colour relation, and were reported to be driven by the u band, which has no influence on equation (3).

2.2 Galaxy formation models & lightcones

2.2.1 *The* GALFORM *model*

We compare our observations to a semi-analytic galaxy formation model called GALFORM. The GALFORM model was first presented in Cole et al. (2000), but it grew from a number of previous attempts to model galaxy formation. These models all assume galaxies form in dark matter haloes, and then use analytical prescriptions to approximate key galaxy formation processes (e.g. White & Rees 1978;

[1] http://classic.sdss.org/dr7/algorithms/photometry.html, accessed 19/8/14

Table 1. Summary of the different GALFORM models mentioned in this paper.

Model	Parent model	Cosmology	Key features
Baugh et al. (2005)	Cole et al. (2000)	*WMAP*1	Different IMFs in starbursting galaxies.
Bower et al. (2006)	Cole et al. (2000)	*WMAP*1	AGN feedback in hydrostatic haloes.
Lagos et al. (2012)	Bower et al. (2006)	*WMAP*1	New star formation law accounting for fraction of hydrogen in molecular state.
G14: Gonzalez-Perez et al. (2014)	Lagos (2012)	*WMAP*7	Updated cosmology.
L14: Lacey et al. (in preparation)	Baugh et al. (2005) & Lagos et al. (2012)	*WMAP*7	Combines varying IMF and new star formation law.

White & Frenk 1991; Kauffmann, White & Guiderdoni 1993; Cole et al. 1994). The first GALFORM model has prescriptions for the cooling rate of gas in dark matter haloes, a star formation rate based on available cold gas content, the attenuation of star formation by supernovae feedback and the merging of satellite galaxies to the main galaxy (Cole et al. 2000). Many of these prescriptions have free parameters, controlling factors like the strength of supernovae feedback, that account for complicated physics not fully understood or analytically described. These parameters are tuned such that the model fits a set of observational constraints at low redshift. None of the models used here were tuned to reproduce clustering measurements.

The models require the history of when a dark matter halo formed and merged, sometimes called a halo's 'merger tree' (Lacey & Cole 1993). For this purpose, the models we present here use an *N*-body simulation based on the Millennium Simulation (Springel et al. 2005), but run in the more up-to-date *WMAP*7 cosmology (Komatsu et al. 2011).

2.2.2 *Model lightcones*

The positions and velocities of particles in the simulation are output at epochs spaced in expansion factor, hereafter 'snapshots'. Mock catalogues of galaxies from GALFORM runs on the *N*-body simulation are produced using the code of Merson et al. (2013). This works by interpolating between the snapshots to find the positions of galaxies when they enter the simulated observer's lightcone, i.e. when the light from the galaxy reaches the observer.

From the simulations 26 realizations of each model were created by changing the position and orientation of the virtual observer.[2] These multiple realizations allow us to improve our understanding of sample variance (Section 3.3), and minimize its effect on predictions by plotting mean measurements from the mock realizations (Section 4). One downside is the simulation used has a limited volume, $12.5 \times 10^7 (\mathrm{Mpc}\, h^{-1})^3$, as such the upper-intermediate and highest redshift slices will oversample, over 26 realizations, the simulation by at least a factor of 3 and 8. Note this is the total oversampling when you consider a sum over all the realizations, an individual realization is much smaller than the simulation box. Also mitigating this effect is the fact that the location and orientation of the observer is randomly assigned, in this way repeated structures will be observed at different redshifts and orientations, and be sampled by different galaxies. In the lower intermediate redshift slice, the volume of the 26 realizations is only 4 per cent larger than the simulation, which should result in very little oversampling. How the oversampling affects results will be discussed in later sections.

[2] These mock catalogues will be made available from the VirgoDB: http://icc.dur.ac.uk/data/ (Lemson & the Virgo Consortium 2006)

The next sections describe the specifics of the two versions of GALFORM we consider. A summary of the relevant GALFORM models can be seen in Table 1.

2.2.3 *The G14 model*

The Gonzalez-Perez et al. (2014, G14) model has the same physical prescriptions as the Lagos et al. (2012) model, which is itself an extension of the Bower et al. (2006) model. The Bower et al. (2006) model added AGN feedback to the Cole et al. (2000) model in order to better reproduce galaxy colours, and to decrease the number of galaxies predicted to lie in the bright end of the luminosity function. The Lagos et al. (2012) model made the star formation rate in the disc of the galaxy proportional to the fraction of the gas that was molecular, by using the empirical star formation law of Blitz & Rosolowsky (2006, see Lagos et al. 2011, 2012 for details).

The update of the G14 model over Lagos et al. (2012) is that it uses merger trees from *WMAP*7 cosmology. *WMAP*7 cosmology has $\sigma_8 = 0.81$, this is smaller than in the *WMAP*1 cosmology of Lagos et al. (2012, $\sigma_8 = 0.9$), so free parameters in the physical prescriptions had to be retuned (Gonzalez-Perez et al. 2014). Tunable parameters were adjusted in order for the predictions to still match the rest-frame b_J and *K*-band luminosity functions at $z = 0$, and give reasonable evolution of the UV and *K*-band luminosity functions (Gonzalez-Perez et al. 2014).

The G14 model converts from star formation history and the initial mass function (IMF) to an SED using an updated version of the SPS model from Bruzual & Charlot (1993).

2.2.4 *The L14 model*

The L14 model also combines the improvements to star formation rate calculations made in the Lagos et al. (2012) model and the AGN feedback model of Bower et al. (2006). It was also run on the new *WMAP*7 *N*-body simulation. Another difference of the L14 model is its IMF. The G14 model uses a Kennicutt (1983) IMF for all stars formed. The L14 model instead adopts a top-heavy IMF in starbursting galaxies, as developed in, but less extreme than, the Baugh et al. (2005) model. This change was motivated to bring the predictions of sub-mm galaxy number counts into closer agreement with observations (Baugh et al. 2005).

A further difference in the L14 model which could have an impact on clustering predictions is the treatment of merging satellite galaxies. The models we present here all use an analytic approximation, from Cole et al. (2000), to calculate how long it takes for an accreted satellite to merge with the central galaxy. This approximation assumes satellites enter the halo on orbits randomly selected from the distribution of satellite orbits given in Tormen (1997), before the orbit decays due to dynamical friction. The Cole et al. (2000) method calculates the time for the orbit to decay using

the formula for Chandrasekhar dynamical friction in an isothermal sphere given in Lacey & Cole (1993). The L14 model, on the other hand, uses the Jiang et al. (2008), Jiang, Jing & Han (2014) formula for the time-scale. The formula has been empirically modified using *N*-body simulations in order to account for the tidal stripping of the accreting haloes. Note that Campbell et al. (2015), motivated by the work of Contreras et al. (2013), additionally develops the model to track the positions of accreted subhaloes in the simulation, rather than using an analytic approximation. We do not attempt modifications to the models in this paper as our focus is on presenting and interpreting the observations.

A final difference between this model and G14 is the adoption of the Maraston (2005) SPS model, which differs from the Bruzual & Charlot (1993) model in its treatment of thermally pulsating asymptotic giant branch stars (TP-AGB). These stars are important in the near-IR. The near-IR corresponds to the *r* and *i* bands we use for luminosity and colour measurements (Maraston 2005).

Note that the version of the L14 model we use is slightly different to more recent versions of the L14 model. The differences are tiny, however, and should not have any impact at the redshifts we consider.

2.2.5 *Model stellar masses*

We take stellar masses from the model, but rescale them by $h = 0.702$ (the model cosmology) in order to convert the physical units of the model, $\mathrm{M}_\odot\, h^{-1}$, to the units of the observations, $\mathrm{M}_\odot\, h^{-2}$. Mitchell et al. (2013) demonstrates that applying broad-band SED fitting to model galaxy photometry can give a biased estimate of the true model galaxy's mass. In order to investigate what effect this may have we show the inferred mass, from equation (3), against the true model mass in Fig. 1. In G14, the relation between true and observed mass has a gradient, leading to smaller masses being systematically underpredicted by the model. Red galaxies in G14 tend to be affected by this more than blue galaxies. In L14, the differences in mass have a larger scatter, the blue galaxies still show a gradient but the inferred mass is now generally an overprediction of the true mass. The scatter between the inferred and true mass is also larger for the L14 model. Applying the colour relation to estimate mass, as compared to using the true mass, can cause both the masses and the typical colours of galaxies to change in the sample. Campbell et al. (2015) demonstrate these differences can affect the clustering signal, with the effect being particularly marked for the L14 model. In this paper, we take the model masses at face value, except for a small adjustment explained in Section 2.3.3. We discuss the possible effects of this when interpreting results.

2.2.6 *Literature* GALFORM *comparisons*

The GALFORM model has been compared to a variety of observational measurements, including those made from this GAMA sample. Indeed several of the GALFORM models were created to address a disagreement with observations. For example, Kim et al. (2009) compared the Bower et al. (2006) and Font et al. (2008) models to 2dFGRS data and found that the model predictions for the dependence of clustering on luminosity were not successfully reproduced. Kim et al. (2009) also found that the model had excess small-scale clustering. The authors put this down to the Bower et al. (2006) model having too many satellite galaxies.

In support of this, McNaught-Roberts et al. (2014) compares the luminosity function as a function of environment of the Bower et al. (2006) mocks to those of GAMA galaxies, and finds an excess of faint, red galaxies in the model. Robotham et al. (2011) additionally found an excess of high-multiplicity (10 or more galaxies) groups in the Bower et al. (2006) model compared to the GAMA data.

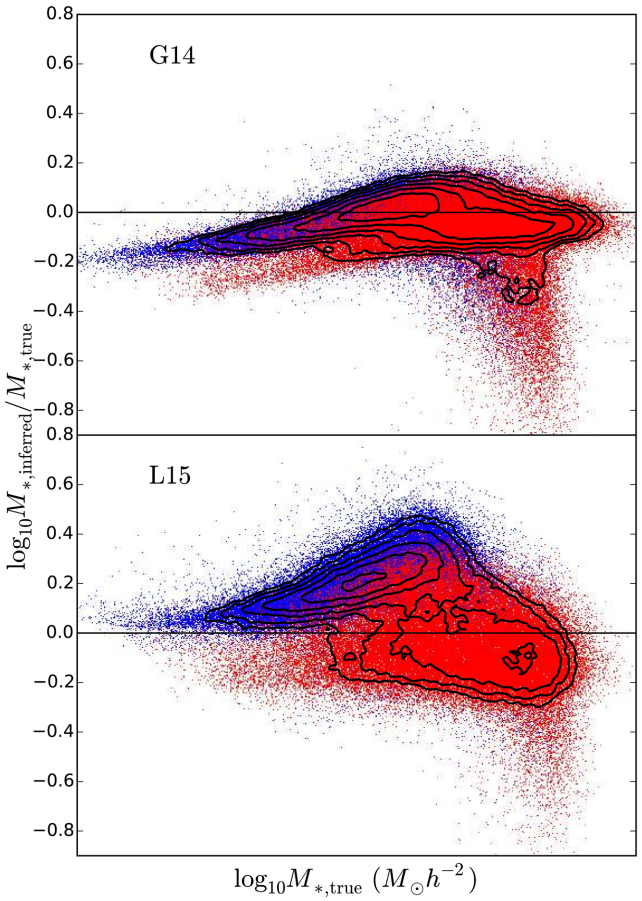

Figure 1. The inferred mass, from the Taylor et al. (2011) colour-to-mass relation, versus the true mass of mock galaxies, for the G14 (top) and L14 (bottom) models. The red and blue points represent red and blue galaxies, as selected by our colour cuts (Section 2.3). The contours are spaced evenly in log-space, between 5×10^4 and 50×10^4 galaxies dex^{-2}. Inferring the mass using observational relations, rather than using the true model mass can make a significant difference and is in this context model dependent.

Campbell et al. (2015) combine SDSS and VIPERS measurements with the ones presented here to compare the clustering of galaxies as a function of stellar mass to that predicted by a variety of GALFORM versions, across several different epochs. They find good agreement between the models and data, but in order to fit small-scale clustering they have to adopt a new, hybrid model for satellite orbits. In this model, satellites follow resolved subhaloes and an analytic merger time-scale is only computed once the subhalo is lost.

Their paper focuses on how different methods of estimating stellar mass affect clustering measurements; our paper takes the complementary approach of comparing a wider range of galaxy properties. In addition, our paper utilizes the lightcone modelling of Merson et al. (2013), whilst Campbell et al. (2015) uses clustering of galaxies in a single, constant cosmic time, snapshot.

2.3 Sample selection

2.3.1 Redshift slices

We want to study the evolution of galaxy clustering with luminosity, mass, colour and redshift. One approach to this is to use volume-limited samples, which are characterized by a uniform detection probability across the sample volume. However, volume-limited samples reduce the amount of data available for the analyses, so we also consider magnitude-limited samples. In order to do this, we ensure the survey's radial selection function is properly dealt with by the random catalogue (see Section 3.1). Using magnitude-limited samples means interpreting the results requires consideration of the selection function, but offers the most powerful test of the model. We separate all of our mass, luminosity and colour samples into four redshift bins: low-z, $0.02 < z < 0.14$, intermediate-z, $0.14 < z < 0.24$, upper intermediate-z, $0.24 < z < 0.35$ and high-z, $0.35 < z < 0.5$. The volumes of these slices are 1.2×10^6 (Mpc h^{-1})^3, 5.0×10^6 (Mpc h^{-1})^3, 1.3×10^7 (Mpc h^{-1})^3 and 3.7×10^7 (Mpc h^{-1})^3, respectively.

In order to help differentiate between selection effects and galaxy formation effects, we also produce samples with upper redshift cuts that have been decreased in order to make the sample essentially volume-limited (comprise of at least 98 per cent of galaxies with maximum observable redshifts greater than the sample limit).[3]

2.3.2 Luminosity, mass and colour cuts

Luminosity samples are produced from equation (1) with the measured SDSS r-band DR7 Petrosian magnitude used to calculate the absolute magnitude in the r-band, $M_{r,h}$. Loveday et al. (2015) measures the luminosity function, and finds the characteristic 'knee' of the function at $M^*_{r,h} = -20.6$; past this magnitude the number density of galaxies rapidly drops. This characteristic magnitude lies in our $-21.0 < M_{r,h} < -20.0$ sample, and we measure one sample of galaxies brighter than this and three fainter.

Stellar mass is more complex to compute from observations, but is less complicated to predict from models. We use mass bins of 0.5 dex in size, except for the lowest mass sample, where we increase the bin limits to have more galaxies. Baldry et al. (2012) found for GAMA data at $z < 0.06$ that the characteristic knee of the mass function is at $M^* = 10^{10.35}\,\mathrm{M}_\odot\,\mathrm{h}^{-2}$. This characteristic mass falls into our middle mass bin, we use two samples less massive and two samples more massive than this.

In addition to luminosity and mass samples, galaxies are divided into a red population and a blue population. The colour of a galaxy is often used as a rough proxy for the age of its stellar population, with galaxies undergoing star formation generally being expected to be bluer. It is therefore interesting to study how clustering differs as a function of colour. In Fig. 2, we show the colour–magnitude diagram for our flux-limited ($r < 19.8$) sample of galaxies. We use a sloping cut with a gradient of 0.03, following the typical literature values (e.g. Bell et al. 2003),

$$(g-r)_0 = -0.030 * (M_{r,h} - M^*_{r,h}) + 0.678. \quad (4)$$

[3] Applying the same cuts to the mock catalogues leads to a larger fraction of some mock samples being magnitude-limited, at worse the volume-limited fraction is 89 per cent. Clustering from a mock catalogue for samples even more magnitude-limited than this (as low as 78 per cent) show no significant differences with the clustering from the same mock with a deeper apparent magnitude cut ($r < 21$). We will therefore treat the mock measurements as volume-limited.

The intercept of this cut is such that there is an equal fraction of red and blue galaxies. We also show in Fig. 2, a volume-weighted colour–magnitude diagram. We see that the volume we observe has an obvious blue cloud, made up of faint galaxies, which is less apparent in the observed colour–magnitude diagram due to selection effects. The colour cut also separates the red sequence and blue cloud in the volume-weighted diagram.

A summary of our cuts and the properties of our samples is given in Table 2.

2.3.3 Cuts and adjustments to the models

When comparing the actual clustering of galaxies to models we want to uncover differences in how dark matter haloes are populated. If we were to apply the same cuts on the models and the data we may get samples with very different number densities, since the luminosities or colours may be incorrectly predicted. Such disagreements are better explored by comparison of model predictions to other observational measurements like stellar mass functions, or colour distributions. In order to focus on the spatial distribution of comparable galaxies in the models and simulations, mock galaxy samples are often selected to have matching number densities to galaxies in the real comparison sample (e.g. Berlind et al. 2003; Zheng et al. 2005; Contreras et al. 2013). We therefore adjust the magnitudes of the mock galaxies in order for the luminosity functions of the mocks and data to match, in each of our four redshift slices.

First, we estimate the galaxy luminosity function of the $r < 21$ unaltered mock magnitudes. We then reassign each galaxy in the mock a magnitude designed to map number densities in the unaltered mock luminosity function to the appropriate magnitude in the data luminosity function. We do this by computing the magnitude difference between the cumulative mock luminosity function and the cumulative data luminosity function at the same cumulative number density. This forces the mock and data luminosity functions to agree. The faint end of the real luminosity functions suffer from incompleteness, as the different k-corrections of the galaxies result in a colour dependence on which galaxies reach the apparent magnitude limit. In order to avoid this, we estimate the complete luminosity function of real data in the three higher redshift slices by switching to the low-redshift real luminosity function past the point where colour-dependent completeness effects become important. The amplitude of the low-redshift luminosity function is scaled to ensure a smooth join with the higher redshift one. The mock catalogue then has an $r < 19.8$ apparent magnitude limit applied to the shifted magnitudes.

We apply the same k-correction polynomials to the mocks, but adjust the limits of the colour bins. This is to ensure the fraction of galaxies in each colour bin is the same as in the data. Thanks to this adjustment, applying the apparent magnitude limit results in a mock catalogue with close to the same selection function as the real data. This is important as many of our samples are magnitude-limited. Unfortunately, unless the mocks have the same colour–magnitude distribution as the data, it is impossible to perfectly model the selection function even with this technique of adjusting the mock k-corrections. This is because the magnitude distribution within a colour bin varies between real and mock data. The masses of the mock galaxies are rescaled to preserve the same mass-to-light ratio. Also note the mock catalogue is fitted with the same P and Q as the data.

We will now describe the cuts for colour selected samples. In Fig. 2, we can see that both models reproduce the bimodality of

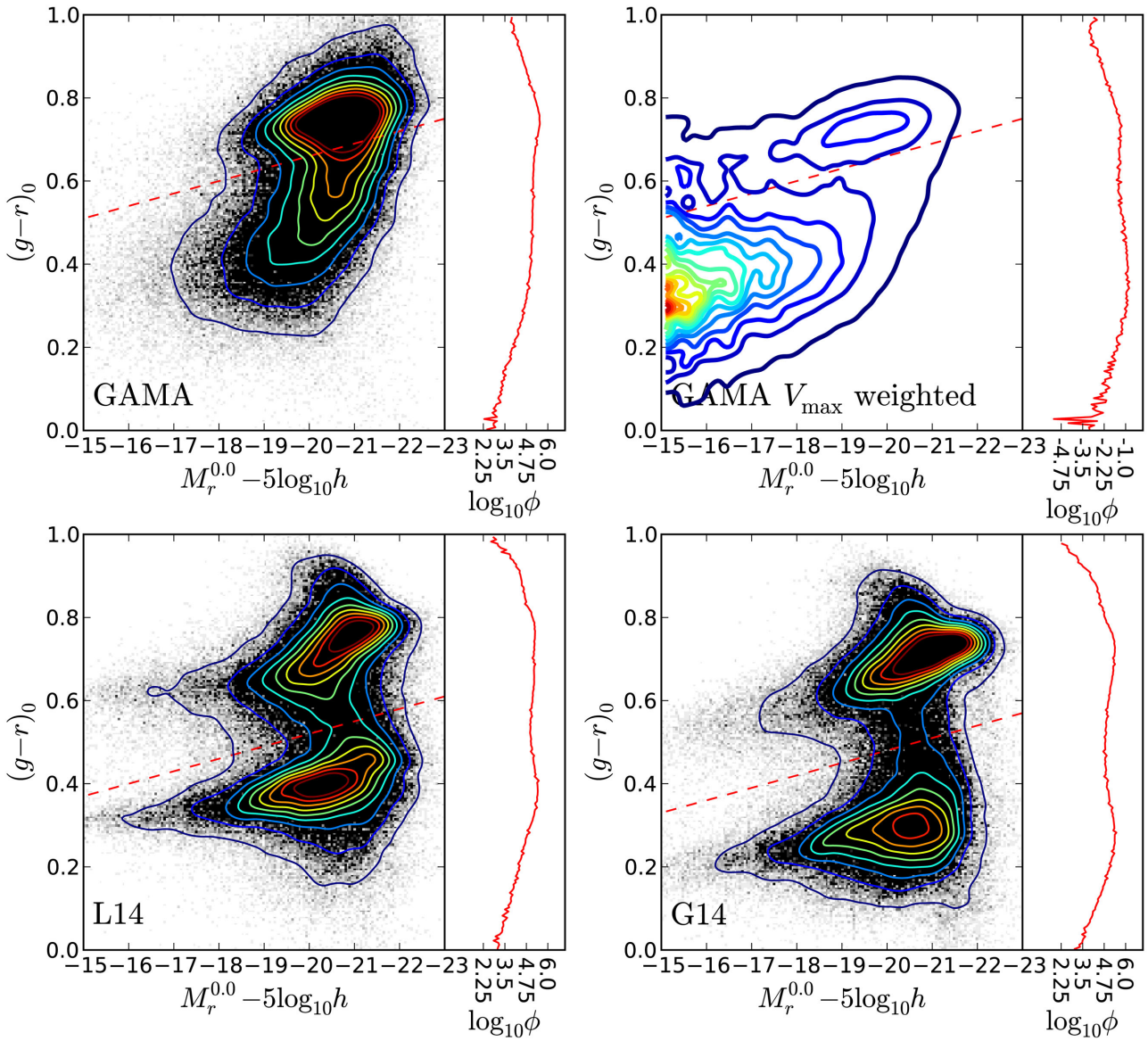

Figure 2. A rest-frame colour–magnitude diagram for the real GAMA galaxies and for the mock galaxies, as labelled. The top-right panel gives the volume-weighted colour–magnitude diagram for the real GAMA galaxies. The red dashed lines shows our cuts to define red and blue samples of galaxies, this cut is different for each model and the data (see Section 2.3.3). A histogram of colours has been added to the right of each panel. Contour levels are spaced linearly, the colour scale is the same in each of the colour–magnitude diagrams, except the volume weighted one. The contours were computed from a binned version of this plot, smoothed with a Gaussian filter.

galaxy colours, but both predict a well-defined blue cloud not seen in the data. Note that whilst the data is flux-limited, meaning faint galaxies may be lost, this selection effect is included in the model lightcone. One suggestion of how to improve the mock galaxy colours was given in Font et al. (2008); here the authors removed the unrealistic GALFORM assumption that all gas is removed from satellites as soon as they accrete on to a halo. By implementing a more realistic model with more gradual removal of gas by ram pressure stripping they found satellites could form stars for longer after being accreted, and ended up with colours between the red and blue sequence. However, the G14 and L14 models do not include any gradual ram pressure stripping.

Looking at the models in more detail, we see the L14 has a redder blue cloud than the G14 model. This is expected as this model uses the Maraston (2005) SPS model which has stronger near-IR emission for young stellar populations. We use the same gradient as the data for the cut, and select the intercept in order to reproduce the observed fraction of red and blue galaxies. For the L14 model this intercept is 0.548, for the G14 model it is 0.498. From Fig. 2, we can see that the cut applied to the models clearly separates the red sequence from the blue-sequence mock galaxies.

In Tables B2 and B3 in Appendix B, the sample sizes and properties for one realization of GAMA are given for the two models.

2.3.4 *Comparison samples*

In addition to the samples we have described, we also produce a sample with which to compare our results to Zehavi et al. (2011). In order to make the comparison samples as similar as possible,

Table 2. Different galaxy samples, sample sizes and median properties. The subscript 'med' indicates the values are medians. Samples with redshift limits marked with asterisks are magnitude-limited, so should be treated with careful consideration of the GAMA selection function. In samples without an asterisk at least 98 per cent of the members are volume-limited. Values in brackets are rms scatter.

Sample	$z_{\rm min}$	$z_{\rm max}$	$N_{\rm gals}$	$z_{\rm med}$	$M_{\rm med}$	$\log_{10}(M_*/{\rm M}_\odot\, h^{-2})_{\rm med}$	$(g-r)_{0,{\rm med}}$
$-18.00 < M_{r,h} < -17.00$	0.02	0.07	2089	0.05	−17.46 (0.28)	8.62 (0.29)	0.42 (0.20)
	0.02	0.14*	5666	0.08	−17.62 (0.27)	8.67 (0.33)	0.41 (0.19)
$-19.00 < M_{r,h} < -18.00$	0.02	0.11	6950	0.09	−18.47 (0.29)	9.13 (0.31)	0.47 (0.21)
	0.02	0.14*	13149	0.11	−18.54 (0.27)	9.15 (0.31)	0.47 (0.19)
	0.14	0.24*	3307	0.15	−18.85 (0.13)	9.26 (0.28)	0.46 (0.16)
$-20.00 < M_{r,h} < -19.00$	0.02	0.14	11741	0.11	−19.47 (0.29)	9.74 (0.29)	0.62 (0.17)
	0.14	0.17	7801	0.16	−19.46 (0.29)	9.74 (0.31)	0.60 (0.22)
	0.14	0.24*	27755	0.18	−19.59 (0.27)	9.79 (0.32)	0.59 (0.20)
	0.24	0.35*	2834	0.26	−19.90 (0.10)	9.81 (0.38)	0.45 (0.18)
$-21.00 < M_{r,h} < -20.00$	0.02	0.14	6945	0.11	−20.40 (0.28)	10.24 (0.25)	0.71 (0.15)
	0.14	0.24	22327	0.20	−20.39 (0.28)	10.27 (0.28)	0.70 (0.15)
	0.24	0.35*	37541	0.28	−20.55 (0.27)	10.39 (0.28)	0.68 (0.17)
	0.35	0.50*	3593	0.37	−20.86 (0.14)	10.42 (0.28)	0.55 (0.16)
$-22.00 < M_{r,h} < -21.00$	0.02	0.14	1843	0.12	−21.27 (0.25)	10.67 (0.19)	0.74 (0.11)
	0.14	0.24	5865	0.20	−21.28 (0.25)	10.70 (0.21)	0.74 (0.13)
	0.24	0.35	15353	0.30	−21.29 (0.25)	10.78 (0.23)	0.74 (0.17)
	0.35	0.37	3168	0.36	−21.28 (0.25)	10.82 (0.23)	0.74 (0.14)
	0.35	0.50*	16114	0.40	−21.42 (0.27)	10.86 (0.28)	0.73 (0.22)
$-23.00 < M^{0.1}_{r,h} < -22.00$	0.01	0.50	2273	0.37	−22.25 (0.19)	11.26 (0.28)	0.79 (0.18)
$-22.00 < M^{0.1}_{r,h} < -21.00$	0.01	0.38	23746	0.29	−21.36 (0.25)	10.79 (0.23)	0.74 (0.15)
$-21.00 < M^{0.1}_{r,h} < -20.00$	0.01	0.26	33965	0.20	−20.47 (0.28)	10.31 (0.28)	0.71 (0.16)
$-20.00 < M^{0.1}_{r,h} < -19.00$	0.01	0.18	22487	0.14	−19.53 (0.29)	9.78 (0.31)	0.62 (0.19)
$-19.00 < M^{0.1}_{r,h} < -18.00$	0.01	0.12	8129	0.09	−18.52 (0.29)	9.16 (0.31)	0.48 (0.21)
$8.50 < \log_{10} M_*/{\rm M}_\odot\, h^{-2} < 9.5$	0.02	0.05	1049	0.04	−17.95 (0.72)	8.88 (0.28)	0.46 (0.15)
	0.02	0.14*	18533	0.10	−18.42 (0.59)	9.07 (0.27)	0.44 (0.13)
	0.14	0.24*	8472	0.17	−19.19 (0.33)	9.32 (0.16)	0.39 (0.10)
$9.50 < \log_{10} M_*/{\rm M}_\odot\, h^{-2} < 10.00$	0.02	0.14	10053	0.11	−19.43 (0.47)	9.74 (0.14)	0.66 (0.12)
	0.14	0.24*	19173	0.18	−19.64 (0.37)	9.79 (0.14)	0.56 (0.12)
	0.24	0.35*	5331	0.27	−20.11 (0.25)	9.84 (0.13)	0.41 (0.11)
$10.00 < \log_{10} M_*/{\rm M}_\odot\, h^{-2} < 10.50$	0.02	0.14	7385	0.11	−20.28 (0.44)	10.21 (0.14)	0.73 (0.12)
	0.14	0.18	7749	0.16	−20.25 (0.43)	10.21 (0.14)	0.73 (0.09)
	0.14	0.24*	23216	0.20	−20.24 (0.40)	10.22 (0.14)	0.72 (0.10)
	0.24	0.35*	23584	0.28	−20.48 (0.29)	10.32 (0.14)	0.63 (0.12)
	0.35	0.50*	3132	0.38	−20.92 (0.26)	10.36 (0.13)	0.48 (0.10)
$10.50 < \log_{10} M_*/{\rm M}_\odot\, h^{-2} < 11.00$	0.02	0.14	2189	0.12	−21.15 (0.38)	10.65 (0.12)	0.76 (0.10)
	0.14	0.24	8018	0.20	−21.10 (0.38)	10.65 (0.13)	0.76 (0.09)
	0.24	0.29	9968	0.27	−21.00 (0.38)	10.66 (0.13)	0.76 (0.09)
	0.24	0.35*	24416	0.30	−21.02 (0.35)	10.68 (0.13)	0.75 (0.09)
	0.35	0.50*	11800	0.38	−21.31 (0.26)	10.78 (0.14)	0.69 (0.12)
$11.00 < \log_{10} M_*/{\rm M}_\odot\, h^{-2} < 11.50$	0.24	0.35	2572	0.31	−21.86 (0.38)	11.10 (0.10)	0.80 (0.15)
	0.35	0.37	698	0.36	−21.74 (0.35)	11.11 (0.11)	0.82 (0.12)
	0.35	0.50*	5962	0.41	−21.81 (0.29)	11.14 (0.12)	0.82 (0.11)
Red	0.02	0.14*	15842	0.11	−19.61 (1.12)	9.98 (0.54)	0.73 (0.17)
$(g-r)_0 + 0.03(M_{r,h} - M^*_{r,h}) > 0.678$	0.14	0.24*	29686	0.19	−20.16 (0.70)	10.26 (0.35)	0.75 (0.14)
	0.24	0.35*	30465	0.29	−20.81 (0.50)	10.62 (0.29)	0.76 (0.15)
	0.35	0.50*	11461	0.39	−21.51 (0.39)	11.00 (0.29)	0.80 (0.23)
Blue	0.02	0.14*	26437	0.10	−18.61 (1.21)	9.11 (0.62)	0.44 (0.12)
$(g-r)_0 + 0.03(M_{r,h} - M^*_{r,h}) < 0.678$	0.14	0.24*	29906	0.19	−19.77 (0.67)	9.74 (0.42)	0.51 (0.11)
	0.24	0.35*	26227	0.29	−20.56 (0.49)	10.26 (0.35)	0.56 (0.12)
	0.35	0.50*	10122	0.39	−21.22 (0.39)	10.61 (0.30)	0.58 (0.12)

we use magnitudes corrected to $z_{\rm ref} = 0.1$ and use the redshift cuts stipulated in Zehavi et al. (2011). These magnitudes will be labelled with the superscript '0.1'. Unfortunately, the Zehavi et al. (2011) redshift cuts greatly restrict the volume of our survey. As such, only two of the Zehavi et al. (2011) magnitude bin samples, $-22.0 < M^{0.1}_{r,h} < -21.0$ and $-23.0 < M^{0.1}_{r,h} < -22.0$ have a large enough volume in GAMA for worthwhile comparison, having volumes of 6.2×10^6 (Mpc h^{-1})$^{-3}$ and 1.6×10^6 (Mpc h^{-1})$^{-3}$, respectively. The redshift cuts for the fainter magnitude bins result in extremely small volumes in GAMA [less than 1.1×10^5 (Mpc h^{-1})$^{-3}$].

We also produce a series of volume-limited samples with which to compare to SDSS, using deeper redshift cuts appropriate to GAMA's fainter selection limit. These samples are included in Table 2.

3 METHODOLOGY

In this section, we will introduce our method to produce random catalogues, before explaining how we compute the 2PCF, $w_p(r_p)$.

3.1 Random catalogues

3.1.1 The Cole (2011) method

To measure clustering, one needs a random set of points with the same radial and angular selection function as the data. We generate catalogues of random positions using the method set out in Cole (2011), which generates random catalogues from the real data in a way that removes the effects of the large-scale structure. We use the Cole (2011) method without the complications of the extended method designed to fit a parametrized evolution model to the galaxies. For each galaxy in the catalogue, the maximum volume of space over which it could be observed, $V_{\rm max}$, is calculated by finding $z_{\rm min}$ and $z_{\rm max}$, the redshift where a galaxy meets the bright and faint magnitude limits of GAMA II. In addition to $V_{\rm max}$, a density weighted maximum volume, $V_{\rm max,dc}$, is calculated as

$$V_{\rm max,dc} = \int_{z_{\rm min}}^{z_{\rm max}} \Delta(z) \frac{{\rm d}V}{{\rm d}z} {\rm d}z, \tag{5}$$

where $\Delta(z)$ is the overdensity as a function of redshift and ${\rm d}V/{\rm d}z$ is the comoving volume element per redshift element. Given these volumes, every real galaxy in the catalogue is cloned n times, where n is given by

$$n = n_{\rm clones} \frac{V_{\rm max}}{V_{\rm max,dc}} \tag{6}$$

with $n_{\rm clones}$ being the total number of randoms divided by the number of galaxies in the sample. Our default random catalogues have $n_{\rm clones} = 400$. When cloning the galaxy, all of the intrinsic galaxy properties are also cloned, so that the random points have a stellar mass, an absolute magnitude and a colour. The cloned galaxies are randomly distributed within the real galaxy's $V_{\rm max}$, with the GAMA angular mask used to ensure the angular selection function of the cloned galaxies matches that of the real galaxies.

This method requires the estimation of $\Delta(z)$, which is done using an iterative method. Initially, it is assumed $\Delta(z) = 1$ everywhere such that each galaxy is cloned the same number of times. From this random catalogue, $\Delta(z)$ is estimated from the redshift distribution of the randoms, $n_{\rm r}(z)$, and the data, $n_{\rm g}(z)$, using

$$\Delta(z) = n_{\rm clones} \frac{n_{\rm g}(z)}{n_{\rm r}(z)}. \tag{7}$$

A new random catalogue is then produced with this new estimate of $\Delta(z)$, and the whole process repeated until $\Delta(z)$ converges. We iterate 15 times, and find this is more than enough iterations for the process to converge.

An added bonus of this method is that the $V_{\rm max,dc}$ can be used to easily estimate the luminosity function (Cole 2011). We use this technique when estimating luminosity functions for the purpose of adjusting mock galaxy magnitudes to match the abundance of real galaxies. A study of the luminosity functions of GAMA galaxies from this estimator is given in Loveday et al. (2015).

3.1.2 Windowed clones

As previously mentioned, the creation of this random catalogue requires that one adopt a certain value of Q (equation 1). Additionally, our choice of Q is motivated by our decision not to consider evolution in the overall number density of galaxies. It may be the case that our chosen Q is not true to the data, or some density evolution is present in the sample. To mitigate possible effects from this, we add a new technique to the Cole (2011) method.

The key idea of this method is to restrict the redshift of cloned galaxies to some window function around the redshift of the original galaxy. Evolution is therefore included naturally in the random catalogue, as cloned galaxies are kept close to their original redshift. Hence, the error introduced by the inadequacy of the adopted P and Q model is limited. We choose to define our window as a function of volume, $W(V)$; this is because volume is most closely related to the expected fluctuations in the galaxy $\Delta(z)$. With a window defined in terms of volume, the $n(z)$ is smeared out more in the sample variance prone, low-redshift part of the $n(z)$ and less at higher redshift. We adopt a Gaussian window function, with $\sigma = 3.5 \times 10^6 ({\rm Mpc}\ h)^{-3}$, truncated at 2σ. We found this to be a good compromise between limiting the effects of evolution and smoothing out large-scale structure. We also include this window in the computation of $V_{\rm max}$ and $V_{\rm max,dc}$, by weighting volume slices by the window when numerically computing the integral. When the window function reaches a boundary, either the $V_{\rm max}$ of an object or the limit of the survey, it is reflected from that boundary in order to ensure the randoms are scattered symmetrically across the volume. Simply truncating the window at a redshift limit would result in randoms being artificially more likely to be moved away from the limit. This method will be further explored, along with the choices of σ, in a future paper. We will, however, demonstrate one success of the method here empirically. In Fig. 3, we show the redshift distribution of GAMA cloned galaxies, for different bins of the original galaxy redshift. In the top panel of Fig. 3, we can see that cloned galaxies are spread widely across the full redshift range of the survey. In the bottom panel of Fig. 3, we can see that the addition of a window function has limited the redshift range over which a cloned galaxy can move. As such it has limited the effects of deviations of the evolution away from the description given by the adopted values of P and Q.

This windowing method requires further testing and tuning, to see how successful it is in removing the effects on the random catalogue from unmodelled galaxy evolution. However, for this work we show in Appendix A that the windowing affects our results much less than sample variance.

3.1.3 The resultant catalogue

We show in Fig. 4 (top) the redshift distribution of the data and the randoms for different iterations of this process. We see that using the density-corrected maximum volume (olive and blue dashed line) only introduces subtle differences into the $n_{\rm r}(z)$ of the randoms, as compared to simply using $V_{\rm max}$ (red dashed line). The twelfth iteration (blue) and the fifteenth iteration (olive) agree; this indicates the process has converged. The $n_{\rm r}(z)$ of the randoms is a good fit to the $n_{\rm g}(z)$ of the total sample; later we will check the random $n_{\rm r}(z)$ is appropriate for galaxies split into magnitude, colour and mass samples. Note that it does appear that the random catalogue slightly follows the underdensity at $z \sim 0.22$; we found this was not the case when not using the window function and as such claim this is an unfortunate side effect of the modification to the method

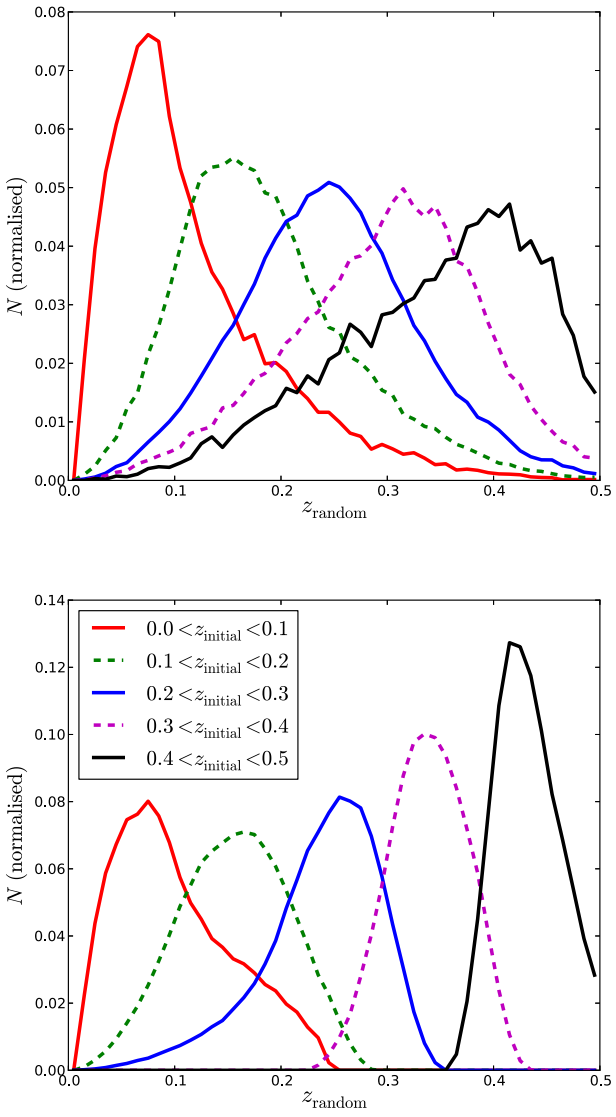

Figure 3. The distribution of the final redshifts of the random points, in bins of their initial redshift, for a random catalogue for the real GAMA data, generated without (top) and with (bottom) the window function update. The window function update acts to limit how far a cloned galaxy can move from its initial position. This in turn limits the effects of any unmodelled galaxy evolution on the random catalogue.

(Farrow 2013). We have, however, tested our clustering results using randoms from the old and new methods, and only find small differences that are at large scales. These differences are a fraction of the error bars, and as such our results will not be significantly affected.

In Fig. 4 (Bottom), we plot the overdensity estimate, equation (7), for successive iterations of our random catalogue generating method. As expected, the iterations act to slightly increase the overdensity estimates, as the Cole (2011) method acts to remove their effect from the random catalogue. This method of generating randoms ameliorates the effects of large-scale structure on the generation of a random catalogue, as overrepresented galaxies from overdense regions are cloned fewer times whilst underrepresented galaxies are cloned more times. Cole (2011) demonstrates how this scheme can produce a random catalogue unbiased by large-scale structure. A strength of this approach to generating randoms is that the random catalogue comes with all of the properties of the galaxy catalogue. One can then apply the same selection to the random catalogues and the galaxy catalogues so that the random catalogue has the correct angular and radial distribution. We intend to make these random catalogues available to the GAMA community via a DMU, which we also intend to distribute to the larger astronomical community once the GAMA data become public.

In Fig. 5, we show the redshift distribution of the randoms and GAMA data, split into samples. We see for the luminosity, mass and colour samples we study the random redshift distribution is an excellent fit to the data.

3.1.4 *Randoms for the mocks*

We apply the same techniques to generate randoms for the mock catalogues. This technique is applied first to the original mock catalogue with unadjusted magnitudes and $r < 21.0$, in order to estimate the mock luminosity function. The technique is applied again to the mock catalogue with adjusted magnitudes and $r < 19.8$, to yield the final random catalogue. We find that the resultant $n(z)$ of the randoms are a good fit to the mock catalogues.

3.2 Projected clustering

We measure the 2PCF of galaxies using pairs of galaxies and randoms with the Hamilton (1993) estimator. Following the standard approach adopted in the literature (e.g. Coil et al. 2008), we measure pair separations parallel, π, and transverse, $r_{\rm p}$, to the line of sight for each pair. These are computed by first converting the angular position and redshift of each object to a vector, $\boldsymbol{r}$. We then define a line-of-sight direction to a pair as $\boldsymbol{l} = (\boldsymbol{r}_1 + r_2)/2$, where $\boldsymbol{r}_1$ and $\boldsymbol{r}_2$ are the positions of the two pair members. The parallel to the line-of-sight distance, π, is the projection of the separation, $\boldsymbol{s} = \boldsymbol{r}_2 - \boldsymbol{r}_1$, on to the line of sight

$$\pi = \frac{\boldsymbol{s} \cdot \boldsymbol{l}}{|\boldsymbol{l}|}. \quad (8)$$

The separation transverse to the line of sight is then

$$r_{\rm p} = \sqrt{|s|^2 - \pi^2}. \quad (9)$$

Pairs are binned on to a grid of π and $r_{\rm p}$. In order to maximize signal-to-noise ratio, we use a mixed linear and logarithmic binning scheme. Bins are linear with 0.0625 h^{-1} Mpc width up to 0.3 h^{-1} Mpc, and are 0.12 dex in size for bins larger than that. Whilst, we generate 400 times as many random points as the data, when computing clustering we use between $n_{\rm clones} = 32$ and $n_{\rm clones} = 200$ times more randoms than data, the number varies in order to maintain good statistics for the samples where the galaxies only sparsely populate the volume.

It is well known that the measured correlation function is distorted by the peculiar velocities of galaxies. On larger scales, the infall of galaxies squash the observed correlation function in the line-of-sight direction (Kaiser 1987). On small scales, the virial motions of galaxies within clusters can elongate the correlation function along the line of sight (Jackson 1972). These distortions have been studied in the GAMA data by Loveday et al (in preparation) and Blake et al. (2013); in this work, we focus instead on the projected correlation function, $w_{\rm p}(r_{\rm p})$. The projected correlation function is a standard approach for dealing with redshift space distortions, which involves

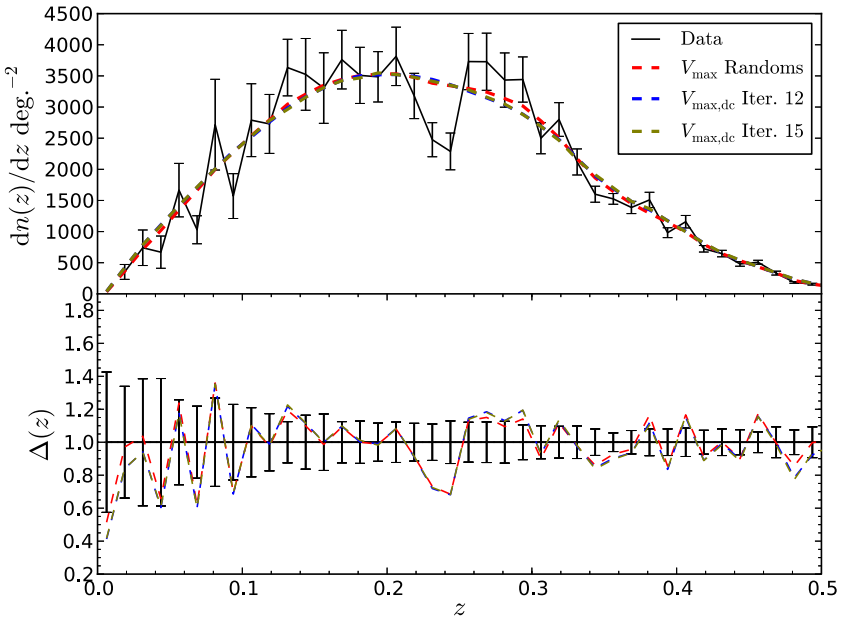

Figure 4. Top: the redshift distribution of GAMA II galaxies (solid) and our randoms (dashed) for multiple iterations of the Cole (2011) random catalogue generating approach (see legend), combined with our window function modifications, as explained in Section 4.3.2. The redshift distribution of the randoms is a good match to the data. Bottom: our estimates of the galaxy overdensity as a function of redshift, from the ratio of the galaxy and random redshift distributions. The error bars are from the rms scatter of the 26 mock realizations, as such they account for the large-scale structure variations. Note these error bars may be underestimates, as the mock realizations oversample the simulation volume at high redshifts.

integrating $\xi(r_\mathrm{p}, \pi)$ along the π direction to minimize their effects, thus

$$w_\mathrm{p}(r_\mathrm{p}) = 2\int_0^{\pi_\mathrm{max}} \xi(r_\mathrm{p}, \pi)\mathrm{d}\pi. \tag{10}$$

In practice, this integral is carried out numerically using our $\xi(r_\mathrm{p}, \pi)$ grid. The choice of π_max warrants careful consideration. Ideally, one would use the largest possible value of π_max to include most of the 2D clustering signal, and because theoretically the effects of redshift space distortions are only removed if you integrate out to infinity. Unfortunately, in real surveys noise affects the measurements, and measurements for large values of π_max can be particularly noisy. We adopt a value of $\pi_\mathrm{max} = 41\,\mathrm{Mpc}\,h^{-1}$ for our measurements, which is a reasonable π_max value to consider for the scales analysed (see e.g. fig. 1 of Norberg et al. 2009). For the Zehavi et al. (2011) comparison sample, we use $\pi_\mathrm{max} = 60\,\mathrm{Mpc}\,h^{-1}$, which makes our measurements noisier but matches the Zehavi et al. (2011) π_max.

The results of equation (10), with $\pi_\mathrm{max} = \infty$, can be calculated analytically for a spherically symmetric power-law correlation function, $\xi(r_\mathrm{p}) = (r_\mathrm{p}/r_0)^{-\gamma}$, where r_0 and γ are constants. The result is

$$w_\mathrm{p}(r_\mathrm{p}) = r_\mathrm{p}\left(\frac{r_0}{r_\mathrm{p}}\right)^{\gamma}\frac{\Gamma(1/2)\Gamma((\gamma-1)/2)}{\Gamma(\gamma/2)}, \tag{11}$$

where Γ is the Gamma Function. We will fit equation (11) to some of our samples in Section 5 in order to measure correlation lengths, r_0. As a power law is not a good fit over the whole 2PCF, we restrict the fit to the scales $0.2\,\mathrm{Mpc}\,h^{-1} < r_\mathrm{p} < 9.0\,\mathrm{Mpc}\,h^{-1}$. To fit, we adopt a least-squares minimization method using the diagonal terms of the covariance matrix. To check how the variation of γ could influence the derived value of r_0, we also fit power laws with a fixed $\gamma = -1.8$. All of the measured values are given in the appendix in Table B1. We see only a small difference between the best-fitting r_0 values where γ is free to vary and where $\gamma = -1.8$. The difference is not large enough to affect our conclusions.

When plotting clustering, we often include a reference power-law line or divide through by this reference power law, w_ref, to allow easier comparison between plots. We use the Zehavi et al. (2011) power-law fit to their $-21.0 < M^{0.1}_{r,h} < -20.0$ sample for this purpose, which has $r_0 = 5.33h^{-1}$ Mpc and $\gamma = -1.81$.

The clustering results in this paper have been cross-checked numerous times to great accuracy against independent clustering analyses.

3.3 Error estimates

To compute error bars on our clustering measurements for GAMA data, nine jack-knife samples (e.g. Zehavi et al. 2002), three per region, are formed by rejecting roughly equal-area regions of data. From this method, the covariance matrix C_{ij}, is calculated, the square-root of the diagonal terms of which give the error bars. Work such as Guo et al. (2014) show that with large surveys like SDSS, a large number of jack-knife resamplings ($\sim$100) can give reliable estimates of the covariance matrix. Our smaller area, necessitating a smaller number of jack-knife regions, means we should further test our covariance matrix estimates.

We also test how unbiased using jack-knife errors is for our sample. For this, we utilize the 26 realizations of each model, created by considering different lightcones through the simulation. These estimates of the error should be more realistic, as they are built from a series of lightcones which together sample a larger volume than the GAMA data, even though they are drawn from a single simulation. This latter fact implies that the mock errors shown are likely underestimates of the true sample variance, as estimated from an series of lightcones constructed from independent simulations. We computed the jack-knife errors, for a single mock, and the root mean square (rms) scatter between the different realizations for all of the samples selected on mass. In Fig. 6, we show the ratio of the two error estimates as a function of projected separation.

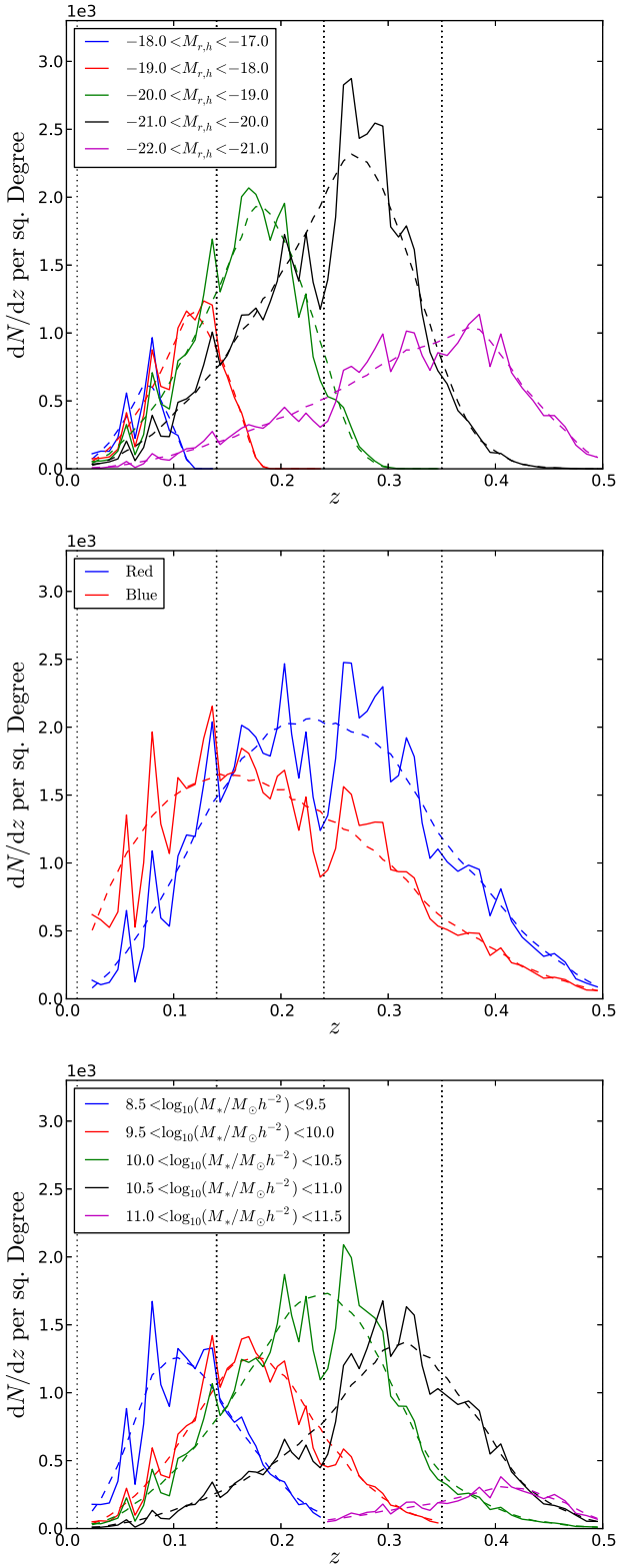

Figure 5. The redshift distribution of the data (solid lines) compared to the redshift distribution of the randoms (dashed lines), for different samples as indicated in the legend. Vertical dotted lines mark the positions of our redshift cuts. The randoms provide an excellent description of the data.

Different colours are from the different models, as indicated. The dashed and solid lines represent two different realizations of the model, encompassing different volumes of the simulation. These two volumes are the same for both models, in order to disentangle the effects of sample variance and galaxy formation.

In the highest redshift slices, the error estimates converge, however note that this convergence could be due to the two realizations sampling some of the same volume of the *N*-body simulation (see Section 2.2.2). In the two lower redshift slices, the realizations should be nearly independent. We can see that for some redshift and mass ranges, the jack-knife errors give the same uncertainty as the model, whilst for others the errors disagree. In particular, the low-redshift jack-knife errors give a lower estimate in the first volume. This suggests that for our samples jack-knife errors could be underestimates at low redshift. As expected, we only see a small difference between the ratios for the two models in the same volume, as such it appears that the ratio is most sensitive to sample variance. Despite the limitations of the jack-knife error estimates with our samples, we use them with the data as it has the advantage of not being model dependent, nor sensitive to how accurately the models reproduce the observed GAMA clustering. However, for the mock predictions we will always plot the error computed from the scatter between the mocks. This is not only true for the clustering measurement, but also for the errors on the parameters of our power-law fits. When we plot the mean correlation functions of our 26 mock realizations, we do not divide our error estimates by $\sqrt{26}$, such that the errors reflect the scatter expected on an individual realization of the GAMA survey. Again recall these errors are underestimates in the two higher redshift slices due to the overlap between lightcones of different realizations in the simulation.

When assessing the goodness-of-fit of the mock predictions to the data, or our data to literature data, we will use the covariance matrix. For the comparisons of our GAMA observations to the literature, we use the covariance matrix from the jack-knife resampling. As we compare to the SDSS measurements of Zehavi et al. (2011), we can disregard the contribution of the errors on the literature measurements to the goodness of fit as they come from a much larger volume than our GAMA samples. When comparing the mocks to the data, we use the covariance matrix computed from the 26 mock realizations. This tests the hypothesis that the data is a realization of the mock. As with the SDSS measurements, the error on the mean measurements from the 26 mocks are small compared the real data uncertainties and are therefore disregarded.

The computation of the inverse of the covariance matrix, C_{ij}^{-1}, can cause problems as our estimates of the covariance, from a limited number of resamplings or realizations, can be noisy. Our method to correct for this follows Gaztañaga & Scoccimarro (2005) and Marín et al. (2013). We first compute the correlation matrix,

$$\tilde{C}_{ij} = \frac{C_{ij}}{\sqrt{\sigma_i \sigma_j}} \tag{12}$$

where σ_i is the standard deviation of the ith 2PCF measurement and i and j are indices running over all of the 2PCF measurements. We then carry out a singular value decomposition (SVD) of it, yielding $\tilde{\mathbf{C}} = \mathbf{U}\tilde{\mathbf{C}}_{\rm SVD}\mathbf{U}^{\rm T}$, where $\mathbf{U}$ and $\mathbf{U}^{\rm T}$ are rotation matrices and $\tilde{\mathbf{C}}_{\rm SVD}$ is a diagonal matrix with elements $\lambda_{ij}^2\delta_{ij}$. The rotation matrix acts to transform the data points into a coordinate system where they are no longer correlated. The basis of this new coordinate system are the eigenvectors of the covariance matrix, given by the columns of the matrix $\mathbf{U}$, which have $\lambda_{ij}^2\delta_{ij}$ as their eigenvalues. As explained in Gaztañaga & Scoccimarro (2005) the eigenmodes of the data

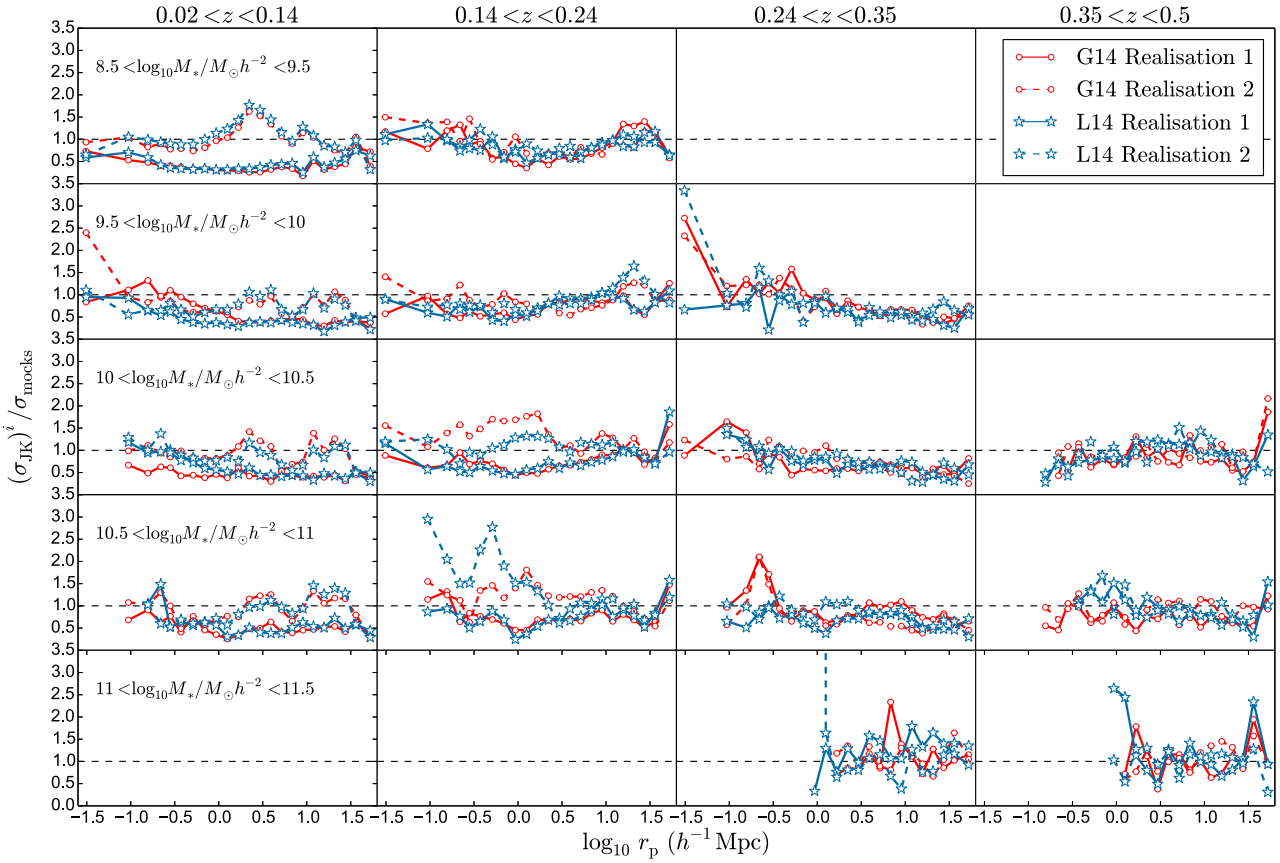

Figure 6. The ratio of error computed from the scatter between 26 mock realizations, and jack-knife error estimates from two different realizations. Red lines are from the L14 model whilst blue lines are from the G14 model. We can see the error estimates from jack-knife resampling can be very different to those from the mock realizations.

expressed in this basis should be uncorrelated, Gaussian distributed and given by

$$\hat{W}(i) = \Sigma_j U_{ji} \frac{W(j)}{\sigma_j}, \tag{13}$$

where $W(j)$ are elements of a vector of the 2PCF measurements, and $\hat{W}(i)$ are the new eigenmodes. As we have a noisy estimate of the covariance matrix, from a limited number of jack-knife samples or mock realizations, some of the eigenvectors will be poorly estimated and using them would bias the estimated χ^2. We would expect the modes which contribute least to the variance to be most likely to suffer from this problem; these modes have small eigenvalues.

We experimented with applying the Gaztañaga & Scoccimarro (2005) cut of $\lambda_{ij} > \sqrt{2/N_{\rm mock,jk}}$ where $N_{\rm mock,jk}$ is either the number of mock realizations for the χ^2 tests of the model ($N_{\rm mock,jk} = 26$), or the number of jack-knife resamplings for the χ^2 tests of whether our results agree with Zehavi et al. (2011, $N_{\rm mock,jk} = 9$). However, we found that this could, counter intuitively, lead to noisier data sets or data sets with fewer reliable measurements having more accepted modes. We therefore adopted the approach of only taking the four largest modes, which for our data is slightly more conservative than applying the Gaztañaga & Scoccimarro (2005) cuts.

To invert $\tilde{\mathbf{C}}_{\rm SVD}$, we simply take $1/\lambda_{ij}$ for each element, this is correct as the matrix is diagonal. We set $1/\lambda_{ij} = 0$ for eigenvalues failing the cuts. Setting values to zero in this way means some possible degrees of freedom are removed. We compute χ^2 using the deviations divided by their associated errors, i.e.

$$\chi^2 = \Sigma_{i,j} \frac{(W(i)_{\rm data} - W(i)_{\rm ref})}{\sigma_i} \tilde{C}^{-1}_{{\rm SVD},ij} \frac{(W(j)_{\rm data} - W(j)_{\rm ref})}{\sigma_j}. \tag{14}$$

Here, the 'data' measurements are the measured GAMA 2PCF and the 'ref' measurements are either literature data or the 2PCF prediction from the combined mock catalogues. As our χ^2 values are still likely to be somewhat inaccurate, we will only indicate whether the cumulative χ^2 distribution for four degrees of freedom suggests a probability of a certain measurement is less than 2 per cent, demonstrating it shows highly statistically significant differences.

4 RESULTS

4.1 Comparison to literature results

In this section, we compare our measurements to those of Zehavi et al. (2011), which come from the SDSS. This comparison acts as a test that our methods for k-correcting galaxies, producing randoms and measuring clustering give reasonable results. We can also use the large area of the SDSS to gauge if the GAMA volume is particularly underdense or overdense.

In Fig. 7, we show our measurements (blue) against those of Zehavi et al. (2011) (black), both for the same redshift cuts. We also show, in red, our measurements for deeper volume-limited samples using the GAMA apparent magnitude limit in Fig. 7.

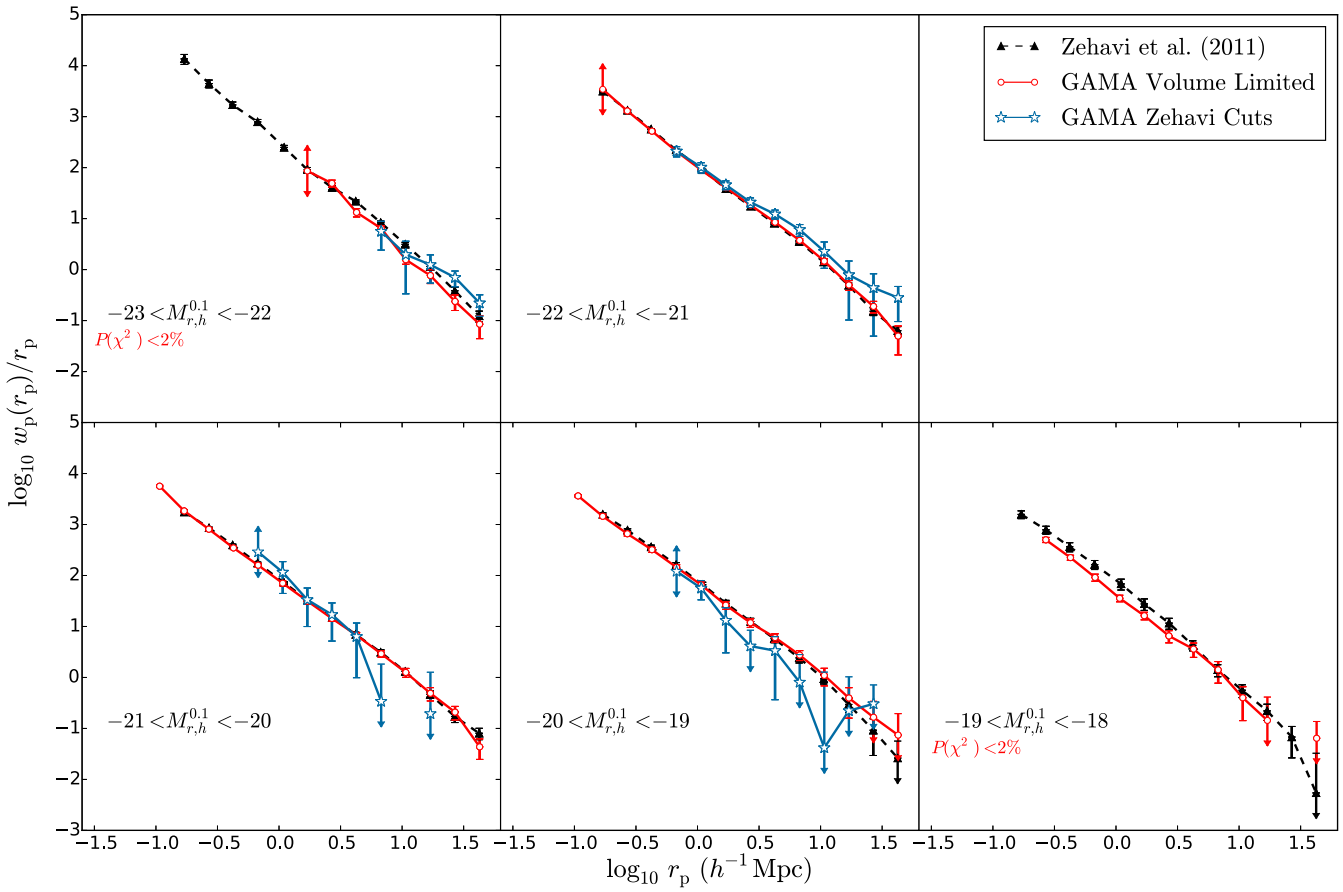

Figure 7. Clustering measurements from Zehavi et al. (2011, black), along with our measurement of clustering for the same magnitude and redshift cuts (blue) and for our, deeper volume-limited samples (red). Error bars are from jack-knife resamplings of the data. As GAMA has a smaller area than SDSS, applying the same magnitude and redshift cuts as Zehavi et al. (2011) resulted in the fainter samples being too small to measure clustering. Where the probability of our data being a realization of the Zehavi et al. (2011) data falls to less than 2 per cent, this is indicated on the panel with the label $P(\chi^2) < 2$ per cent, colour coded by the sample tested. The measurements using the same redshift limits as Zehavi et al (2011) all pass this criteria.

When the probability of the hypothesis that these measurements agree with Zehavi et al. (2011) falls below 2 per cent, it is indicated on the panel. As a simplification, we do not use the Zehavi et al. (2011) error estimates in this calculation, as our errors are the dominant source of uncertainty. The samples with the SDSS redshift limits show good agreement with the SDSS measurements, suggesting the GAMA volume is not particularly unusual in the redshift ranges probed by these samples.

The majority of our deeper, GAMA volume-limited samples agree with the Zehavi et al. (2011) measurements. The brightest however shows a significant variation compared to the lower redshift Zehavi et al. (2011) measurements. Note, however, that the jack-knife covariance matrices may not be accurate for a sample with such a small size and large Poisson errors. The faintest sample also appears to have a highly statistically significant difference compared to the Zehavi et al. (2011) measurement. Specifically, the clustering signal has a lower amplitude. Note, however, the volume of this sample is even smaller than our low-z slice, for which Fig. 6 demonstrates the jack-knife errors can be underestimates by a factor of $\sim$3. In support of this being just being due to sample variance, Driver et al. (2011) find that the GAMA survey is 15 per cent underdense compared to SDSS DR7 up to $z = 0.1$, and the median redshift of this sample is $z = 0.09$.

4.2 Stellar mass dependent clustering

4.2.1 The full shape of the correlation functions

We will now begin to study clustering as a function of a quantity that requires less modelling in the mocks but more modelling in the data: stellar mass. In Fig. 8, we show the clustering of galaxies as a function of mass, divided by our reference power law. Dividing by a reference power law in this way means our measurements show the square of the galaxy bias, relative to the fiducial power law. Note that not all of the samples are volume-limited, so one should be careful to use Table 2 to characterize the typical masses, luminosities and colours of the samples. Samples that are volume-limited are indicated by a star in Table 2. Samples which are more effected by the magnitude selection are expected to have less clustering than volume-limited samples (Meneux et al. 2008), and are expected to be bluer due to our colour-dependent k-corrections. This can be seen in Table 2, where the higher redshift, more magnitude-limited, samples of a particular magnitude or mass range tend to have bluer median colours. The mocks have been constructed to have the same selection function, so it is fair to compare directly.

In all the redshift slices, we observe more clustering in the more massive galaxy samples. This is only seen in Fig. 8 with volume-limited samples in the lowest redshift slice. However, in the two

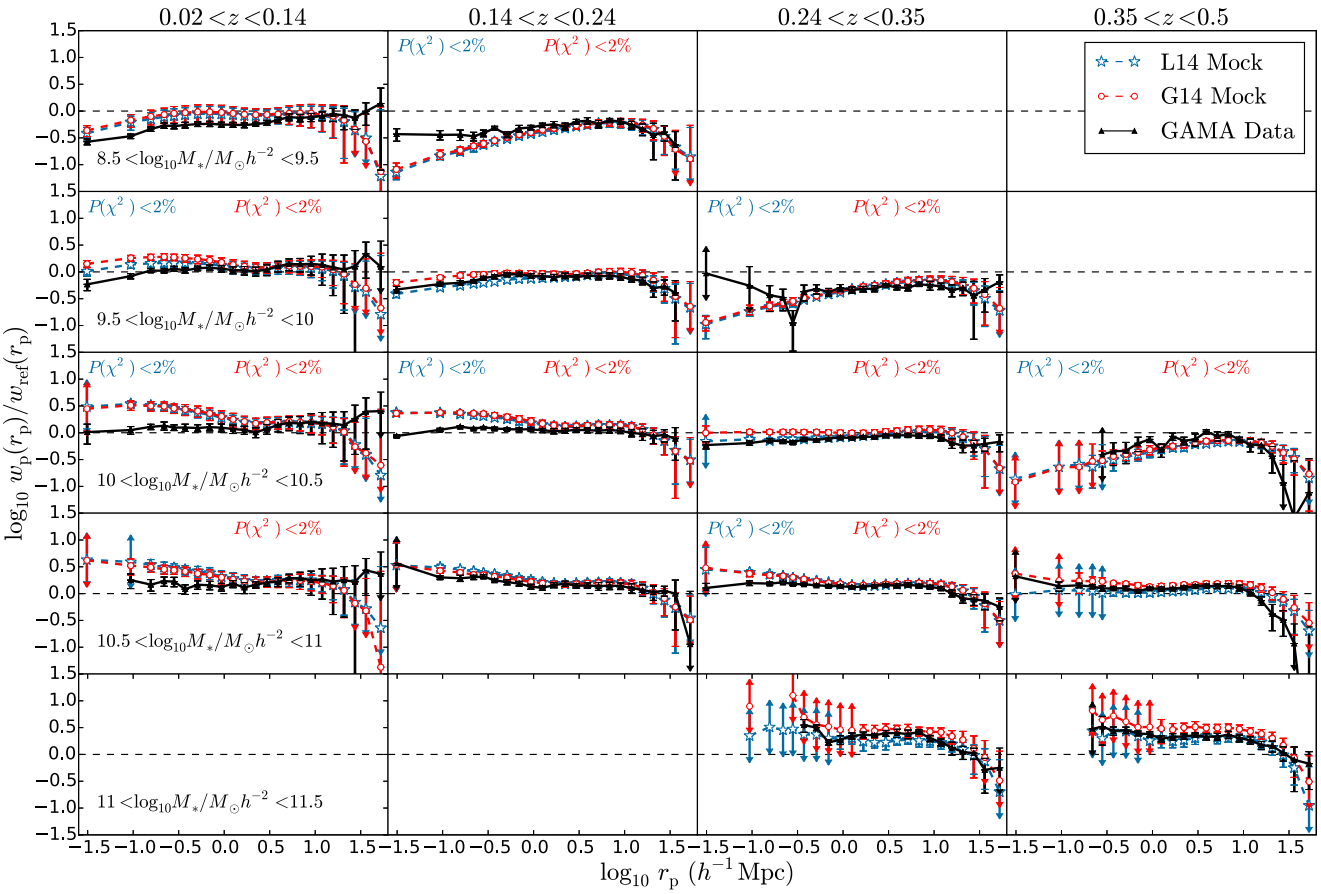

Figure 8. The projected 2PCF of real GAMA (black), G14 model (red) and L14 model (blue) galaxies as a function of redshift (different columns) and stellar mass (different rows). The measurements are divided by the reference power law defined in Section 3.2. Error bars are from jack-knife resamplings for the real GAMA data and the scatter between the mock realizations for the mocks. Marked with $P < 2$ per cent are samples for which the hypothesis that the data is a realization of the model has less than a 2 per cent probability, colour coded according to the model. Despite clustering measurements not being used when creating the models, they reproduce the same trends with mass and redshift as the data. Some samples, however, do show significant differences, particularly on small scales.

highest redshift slices the median colours and magnitudes of the second most massive sample, which is magnitude-limited, are fairly similar to those of the low-redshift volume-limited sample (Table 2). This similarity suggests that the large change in clustering amplitude seen between the $10.5 < \log_{10} M_*/\mathrm{M}_\odot\, h^{-2} < 11.0$ sample and the $11.0 < \log_{10} M_*/\mathrm{M}_\odot\, h^{-2} < 11.5$ sample is real, even though the less massive of these samples is magnitude-limited. In the redshift slices, we also see the small-scale clustering (around $<3\,h^{-1}$ Mpc), relative to the large-scale clustering, increases with mass. This could be interpreted as an increasing fraction of satellite galaxies in the higher mass samples, or it could be a result of fainter, redder satellite galaxies being lost in the more magnitude-limited samples.

The mock predictions for the two models are fairly similar to one another. This similarity suggests the adoption of the Jiang et al. (2008, 2014) approach to computing satellite merger times has only a small effect on the clustering. The general trend of more massive galaxies being more clustered is reproduced. In a ΛCDM cosmology, this implies in both the model and the data more massive galaxies reside in more massive dark matter haloes. As discussed, some of this effect may also be due to using magnitude-limited rather than volume-limited samples. While the amplitude of the clustering in the models is generally an acceptable match to the data, the small-scale clustering is often incorrectly predicted.

For the two slices below $z = 0.24$, galaxy samples in the $10.0 < \log_{10} M_*/\mathrm{M}_\odot\, h^{-2} < 10.5$ mass range appear, by eye, to have too high small-scale clustering. This discrepancy is borne out statistically, with values less than 2 per cent probability of this data being a realization of the model. For the G14 model, this over-prediction of small-scale clustering persists to higher redshift. The mock predictions for the $10.0 < \log_{10} M_*/\mathrm{M}_\odot\, h^{-2} < 10.5$ sample at $0.35 < z < 0.5$ also show a significant discrepancy, which does not appear to be restricted to small scales. However recall that the covariance matrices derived from the mocks are underestimates of the true error in the high redshift slice, due to the oversampling of the N-body simulation.

Additionally, the $8.5 < \log_{10} M_*/\mathrm{M}_\odot\, h^{-2} < 9.5$ sample in the $0.14 < z < 0.24$ slice and the $9.5 < \log_{10} M_*/\mathrm{M}_\odot\, h^{-2} < 10$ in the $0.24 < z < 0.35$ slice has a clustering signal on scales less than a few Mpcs that is significantly too small compared to the GAMA data. This is true even for the latter of those samples, where the data error bars might suggest the model is a good fit. This is because the error bars are much smaller in the mock predictions than in the real data, as the mock number densities are much larger for this sample (recall only the luminosity functions were forced to match).

In Fig. 9, we plot samples which have had their upper redshift limits adjusted in order to make them volume-limited. In general,

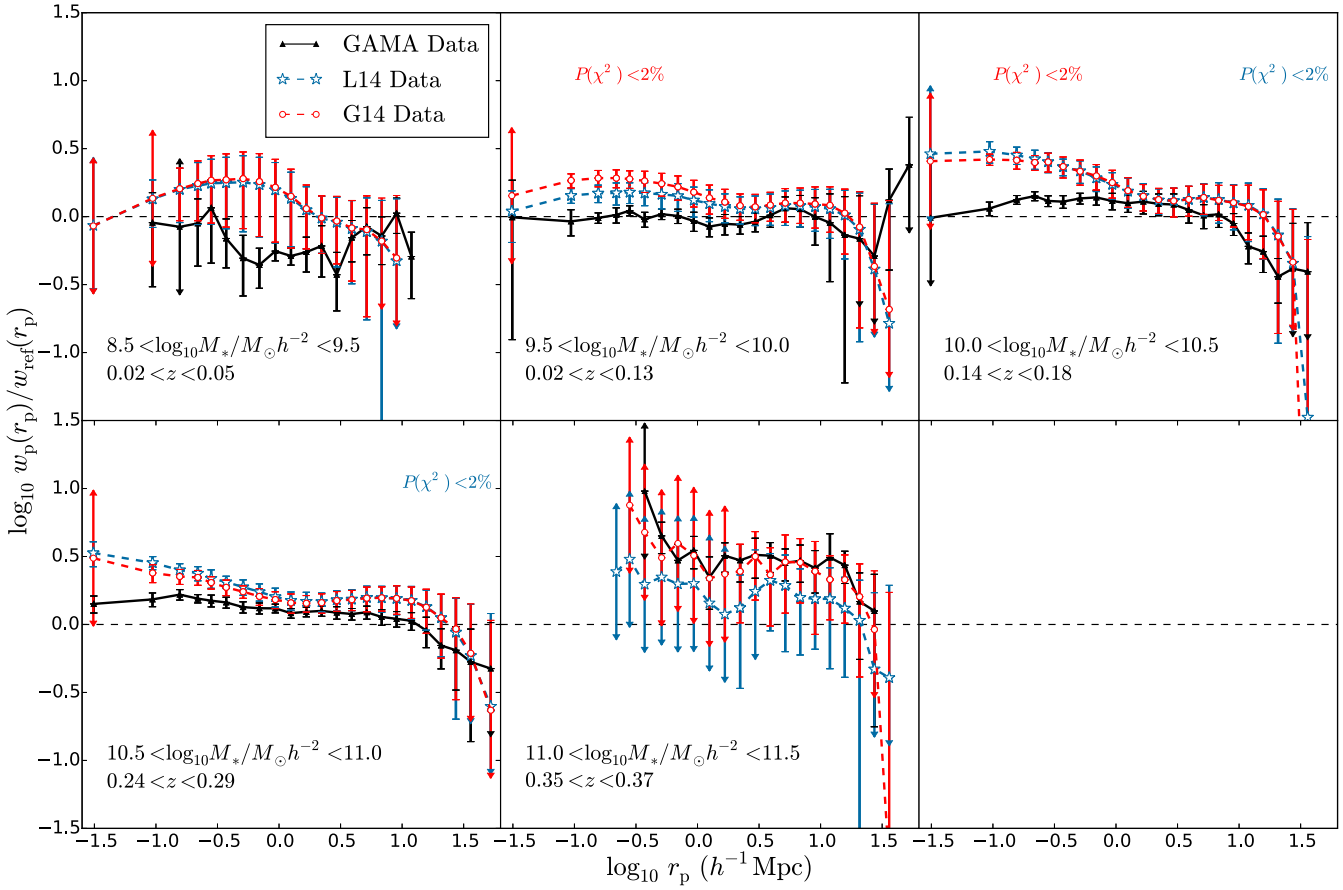

Figure 9. The projected 2PCF of real GAMA (black), G14 model (red) and L14 model (blue) galaxies as a function of stellar mass for different approximately volume-limited redshift slices. The real GAMA samples consist of at least 98 per cent volume-limited galaxies, the mocks 89 per cent. The measurements are divided by the reference power law defined in Section 3.2. Error bars are from jack-knife resamplings for the real GAMA data and the scatter between the mock realizations for the mocks. Marked with $P < 2$ per cent are samples for which the hypothesis that the data is a realization of the model has less than a 2 per cent probability, colour coded according to the model.

they imply the same conclusions as we drew from the flux-limited samples. We again see that the more massive galaxy samples are more clustered. Several of the mock samples have too much clustering on small scales. Seeing this effect in the volume-limited samples means it is not related to the modelling of the selection function.

4.2.2 *Results from power-law fits*

To further investigate the redshift and mass evolution of the clustering, we show in Fig. 10 the r_0 values from the power-law fits to the measurements, as a function of the ratio of the median sample mass to the characteristic mass of the stellar mass function at $z = 0.0$, $10^{10.35}\,\mathrm{M}_\odot\,h^{-2}$ (Baldry et al. 2012). Samples consisting of 95 per cent or more volume-limited galaxies are indicated by a star, magnitude-limited samples are indicated by a triangle. We see very similar dependence of clustering on mass in both the GAMA data and the models. Also, in the magnitude-limited samples of the data and the models, the increase in clustering strength as a function of stellar mass is faster for the higher redshift samples. This effect is also seen in the mock catalogues. This can also be viewed as less massive samples evolving faster with redshift than more massive ones. However, note this effect is not seen when considering the volume-limited samples, which only show weak evidence of redshift evolution.

In order to further explore possible redshift evolution, in Fig. 10 we plot the bias versus mass relation of Li et al. (2006) as dashed lines, colour-coded according to redshift. We convert this relation into r_0 values assuming a power-law correlation function, and calculating the r_0 of dark matter using the bias and r_0 of the galaxy sample containing M_*, i.e. $r_{0,\mathrm{dm}} = r_0(M_*)b(M_*)^{-2/\gamma}$. We can then use the relation $r_0(M) = (b(M))^{2/\gamma} r_{0,\mathrm{dm}}$. We use our own power-law fit to the published Li et al. (2006) sample containing M_* for $r_0(M_*)$. A corresponding bias, $b(M_*)$, is taken directly from the Li et al. (2006) fitting formula. The dashed lines at different redshifts are calculated using the passive evolution model of Fry (1996) to evolve the bias values, and using the growth factor $D(z)$ to evolve the dark matter r_0 as $r_{0,\mathrm{dm}}(z) = r_{0,\mathrm{dm}}(z')(D(z)/D(z'))^{2/\gamma}$. Such a model gives the expected evolution of r_0 for a model where galaxies formed in some density field before moving along trajectories at a velocity defined by their local gravitational potential. The growth factor was calculated for our cosmology from the approximate formula of Carroll, Press & Turner (1992). We assume $\gamma = 1.8$ for the power laws, whilst in reality our value of γ is allowed to vary in the fits. However, we show in Table B1 that using a fixed $\gamma = 1.8$ only has a small effect on our r_0 values.

One clear observation is that in both the volume-limited and magnitude-limited lowest mass sample, the measured amplitude is much lower than the Li et al. (2006) relation. As previously mentioned, GAMA is unusually underdense at low redshifts, and

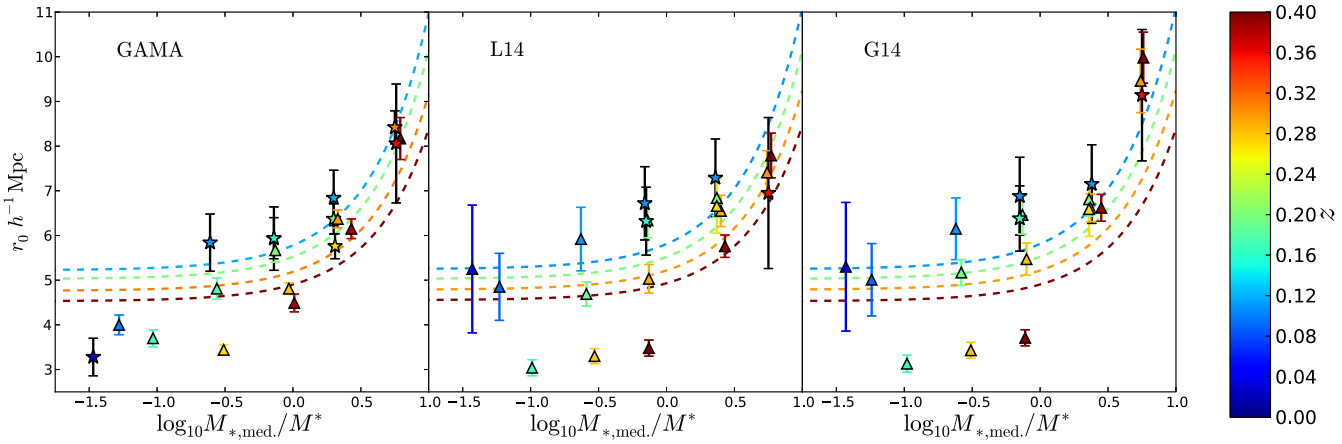

Figure 10. The r_0 of our power-law fits to the range $0.2\,\mathrm{Mpc}\,h^{-1} < r_\mathrm{p} < 9.0\,h^{-1}\mathrm{Mpc}$ as a function of the median stellar mass of the sample divided by the characteristic mass of the stellar mass function (at $z = 0$). The errors come from fitting to the multiple jack-knife regions, or from the scatter from fitting to multiple mocks. Different panels give the GAMA measurements, the L14 model and the G14 model (left to right). Points have been colour coded by median redshift, with samples defined by the same redshift cuts connected by lines. The dashed coloured lines gives the bias fitting formula of Li et al. (2006), converted from bias to r_0 assuming a power-law correlation function with $\gamma = 1.8$ and evolved to different redshifts using the passive evolution model of Fry (1996), more details are given in the text. More massive galaxies are more clustered, a trend qualitatively reproduced by the models. Volume-limited samples are marked with a star, magnitude-limited samples are marked with a triangle. Note the magnitude-limited samples are likely to give lower values of r_0 than the corresponding volume-limited sample. As such the strong trend with redshift for the low-mass samples should not be interpreted as clear evidence of real redshift evolution. This selection effect is accounted for when constructing the model catalogues, so the models and data can be fairly compared.

the jack-knife error bars can considerably underestimate the true uncertainty at low redshift. The very low amplitude in the least massive samples is therefore likely sample variance.

It appears at lower masses the dependence on r_0 with mass is stronger in our data than the fitting formulae. Some of this may be sample variance, but note this strong trend is not seen when only considering volume-limited samples. Indeed the volume-limited samples follow the expected dependence of clustering amplitude with mass. Another likely selection effect is that there is more redshift evolution in the magnitude-limited samples than expected from the passive evolution model. In Fig. 10, we help to mitigate the effect of the GAMA r-band magnitude selection on our results by plotting r_0 against the median mass of the sample. None the less, higher redshift samples will be biased towards different galaxies. As mentioned, more magnitude-limited samples will have lower clustering than volume-limited samples (e.g. Meneux et al. 2008). As such the redshift evolution in clustering amplitude observed in the less massive galaxies may be down to these observational effects. Tests we conducted comparing clustering measurements from $r < 19.8$ and $r < 21$ versions of the mock catalogues support this idea (these samples have a much larger fraction of magnitude-limited galaxies than the samples where we found no significant differences between the original and deeper catalogues).

At higher masses, our measurements are not precise enough to determine if the galaxy clustering is evolving passively or not. It is likely that mass samples in these data can be used to probe redshift evolution, but this may be better done using more sophisticated modelling such as HOD fitting. We leave this to the HOD fitting of Palamara et al. (in preparation), while we focus on comparison to the models which have selection effects included via the use of lightcone.

Returning to the model comparisons then, we see the r_0 values of each model are very similar to one another, except in the high-redshift slice where the L14 model has stronger clustering than the G14 model. The trends seen in the data are also reproduced by both models. In general, the increase of r_0 with magnitude is slightly steeper in the model than the data. The steep increase of clustering with mass, at low masses, is expected to be related to the GAMA selection function. As this trend is qualitatively reproduced by the models, the models have some success in assigning the correct luminosities or colours to the sample galaxies.

4.2.3 Summary of model comparisons for mass samples

To summarize, the most obvious problems with the model predictions as a function of stellar mass are in the one-halo term regime, this points towards the physics of satellite galaxies being a weakness in the model. As mentioned, in Campbell et al. (2015) instead of using the true model masses, they estimate the model masses from the predicted broad-band photometry. They find that this does affect the clustering as a function of mass. The effect is much stronger for the L14 model than the G14 model, and brings the small-scale clustering into better agreement with the data. They still find that even by estimating the masses in this way, the models predict too much small-scale clustering. Also note that the typically redder and fainter satellite galaxies are more sensitive to the r-band apparent magnitude cut (i.e. selection effects), so it may also be related to the model assigning wrong colours or luminosities to satellite galaxies. This is also a possible explanation for the steeper increase in r_0 with mass compared to real data.

4.3 Luminosity dependent clustering

4.3.1 The full shape of the correlation functions

In Fig. 11, we show the clustering of galaxies as a function of luminosity and redshift, in Fig. 12 we show the corresponding volume-limited samples. For all of the redshift intervals, we notice segregation between the faint and bright samples, with brighter galaxies being more clustered. This trend is not seen in the mocks, indeed the clustering of the L14 mock decreases slightly between $-21.0 < M_{r,h} < -20.0$ and $-22.0 < M_{r,h} < -21.0$. Because of this

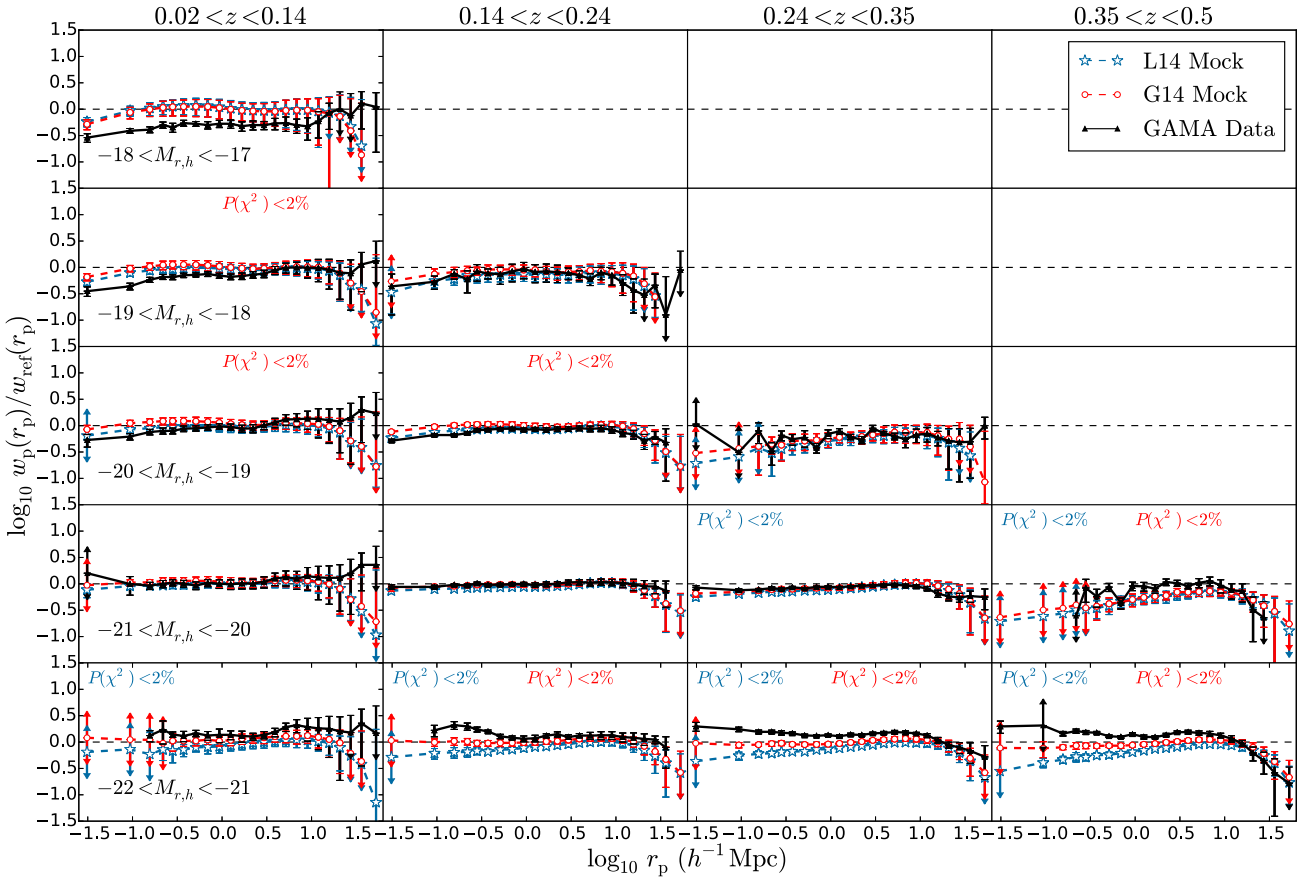

Figure 11. The projected 2PCF of real (black) and G14 model (red) and L14 model (blue) galaxies as a function of redshift(different columns) and luminosity (different rows). The measurements are divided by the reference power law defined in Section 3.2. Error bars are from jack-knife resamplings for the GAMA data, and from the scatter between realizations in the mock. Marked with $P < 2$ per cent are samples for which the hypothesis that the data is a realization of the model has less than a 2 per cent probability, colour coded according to the model. The clustering of faint galaxies is successfully reproduced in the L14 model for the majority of samples. However, the models do not show as much clustering evolution with luminosity as the data, and are particularly discrepant for the brightest sample and on small scales.

lack of dependence on luminosity, the mocks brighter than our sample $-21.0 < M_{r,h} < -20.0$ (which contains $M^*_{r,h}$) all disagree very significantly with the data. For these bright galaxies, the G14 model is closer to the data than the L14 model, but still very discrepant.

For bins fainter than $M^*_{r,h}$, we see good agreement for many of the L14 model samples, in particular for samples fainter than $M_{r,h} = -20$. In contrast, some of the G14 model predictions for fainter luminosity samples show too much clustering on small scales (less than $\sim 3\,h^{-1}$ Mpc). At $0.24 < z < 0.35$ and $-21.0 < M_{r,h} < -20.0$, the L14 model predicts too little small-scale clustering. Additionally, the most luminous mock samples underpredict the clustering, particularly on small scales ($<3h^{-1}$ Mpc) at $z > 0.14$. Apart from this most luminous sample, the small-scale clustering predictions of the mocks are more successful here than in the mass samples. The volume-limited samples in Fig. 12 all show reasonable agreement, given the errors, with the model except the most luminous sample. In this sample, as with the magnitude-limited sample around this redshift, the models underpredict the clustering.

4.3.2 Results from power-law fits

In Fig. 13, we plot the r_0 of our luminosity samples, as a function of the ratio of the median sample luminosity to $M^*_{r,h} = -20.6$ (Loveday et al. 2015). Taking this ratio is useful as it removes a dependence on how magnitudes are converted to luminosities. We see less variation in the clustering properties over this range than we did with mass. Volume-limited samples are plotted with a star, magnitude-limited samples are plotted with a triangle. In Fig. 10, we plot the Zehavi et al. (2011) bias versus luminosity fitting formula as a dashed line, colour coded according to what redshift the relation has been passively evolved. Following Section 4.2.2, to determine the $r_{0,\rm dm}$ needed to convert galaxy biases from the Zehavi et al. (2011) formula to r_0 values, we use the quoted r_0 value from the Zehavi et al. (2011) power-law fit to their sample containing L^*_r as a reference.

Before interpreting these data, we must once more consider the selection effects of the magnitude-limited samples. For these samples the effect is smaller, as the luminosity range is limited in the sample. None the less, because of the colour-dependent *k*-corrections the colours of the samples can change due to the magnitude selection. As before the selection effects may act to artificially enhance any redshift or luminosity trends, by making the clustering of fainter and more distant galaxies appear weaker than it would in a volume-limited sample. This certainly seems to be the case for the most luminous sample in the highest redshift range, where the volume-limited sample has a much larger amplitude than the magnitude limited one at the same redshift. Note the redshift range of the volume-limited sample is very small, and as such it is likely

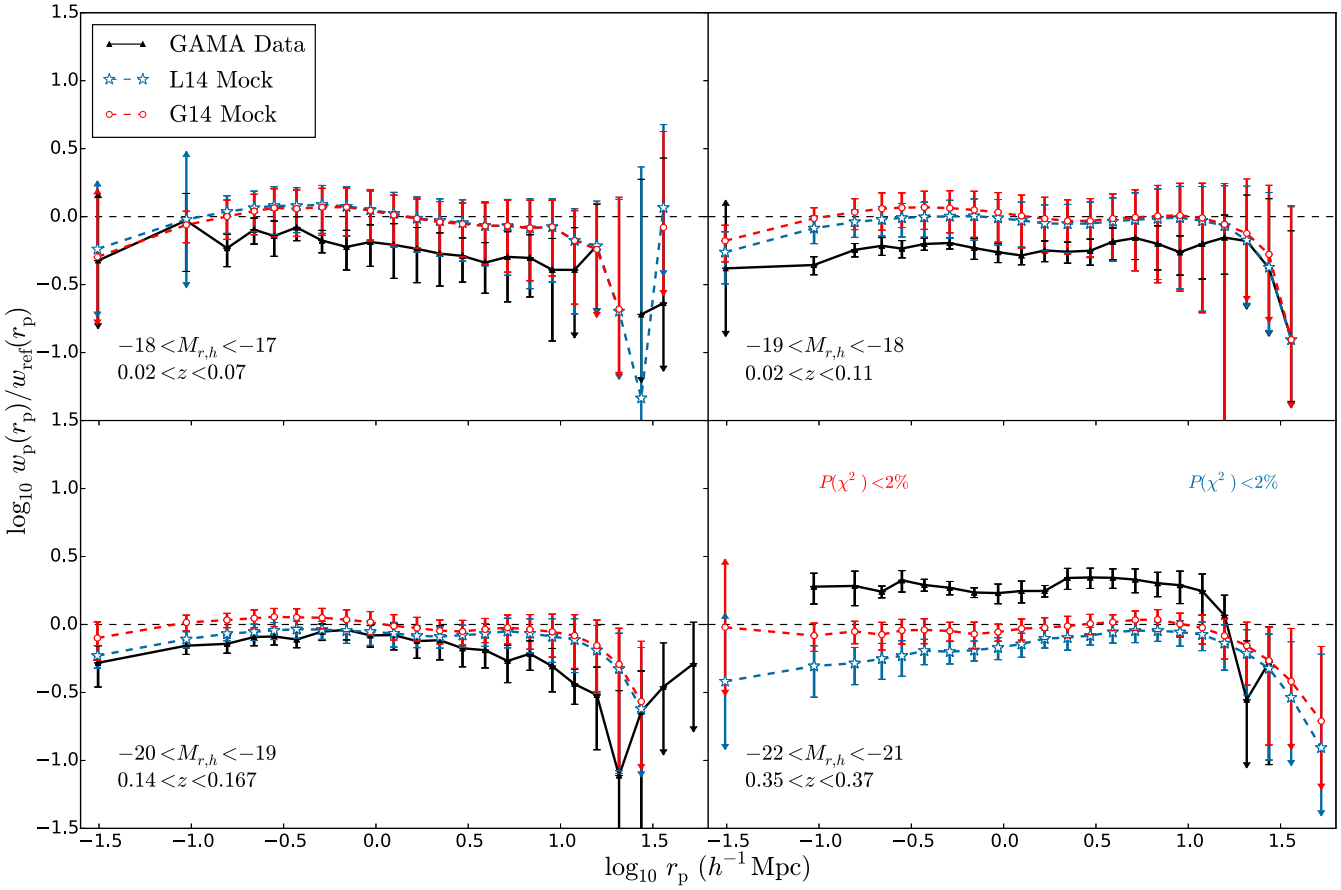

Figure 12. The projected 2PCF of real (black) and G14 model (red) and L14 model (blue) galaxies for different volume-limited luminosity samples. The measurements are divided by the reference power law defined in Section 3.2. Error bars are from jack-knife resamplings for the GAMA data, and from the scatter between realizations in the mock. Marked with $P < 2$ per cent are samples for which the hypothesis that the data is a realization of the model has less than a 2 per cent probability, colour coded according to the model.

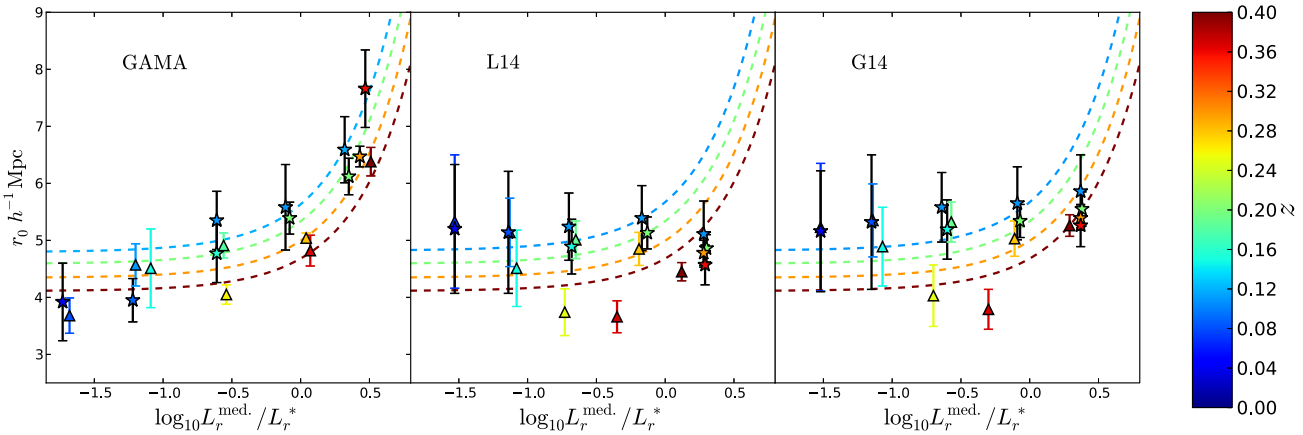

Figure 13. The r_0 of our power-law fits to the range $0.2 < r_{\rm p} < 9.0\,h^{-1}$ Mpc as a function of the median luminosity of the sample, divided by the characteristic luminosity of the data at $z = 0$. Pure luminosity evolution has been accounted for with $Q = 1.45$. The error bars give the error from fitting to the multiple jack-knife regions. Different panels give the GAMA measurements, the G14 model and the L14 model (left to right). Points have been colour coded by median redshift, with samples defined by the same redshift cuts connected by lines. Volume-limited samples are plotted as stars, magnitude-limited samples as triangles. The dashed coloured lines gives the bias fitting formula of Zehavi et al. (2011) with $\sigma_{0.8} = 0.8$, converted from bias to r_0 assuming a power-law correlation function with $\gamma = 1.8$ and evolved to different redshifts using the passive evolution model of Fry (1996), more details are given in the text. The Zehavi et al. (2011) fitting formula is only derived from the range $0.16 < L_r/L_r^* < 6.3$ (Zehavi et al. 2011), but the disagreement at low luminosity is more likely to be down to sample variance underestimated in the jack-knife errors. Brighter galaxies are more clustered in the data, a trend not reproduced in the models. Note the magnitude-limited samples are likely to be underestimates of the true r_0. As such the trends with redshift for the low-luminosity samples should be interpreted with caution (see the text). In the highest luminosity samples, three volume-limited samples demonstrate that r_0 is evolving slower than the passive evolution model (i.e. the bias is evolving faster).

to suffer from sample variance. The r_0 values of the other volume-limited samples seems to roughly agree with the magnitude-limited sample, but note this is for the subset of samples where producing a volume-limited version was possible. It was not possible to construct volume-limited samples for samples with very high fractions of magnitude-limited members, where selection effects are likely to be largest.

The data show an increase in clustering with luminosity in all of the redshift slices. This is seen in many of the volume-limited samples, and so cannot solely be down to selection effects. Unfortunately, as with the mass samples, this trend cannot be confirmed in the two highest redshift slices with volume-limited samples. Except for the lowest luminosity sample, our measurements from real GAMA data agree with the Zehavi et al. (2011) relation in the lowest redshift slice, which is close to the redshift at which the relation was measured. Our lowest luminosity measurement falls well below the Zehavi et al. (2011) relation. As with the lowest mass sample, because we know GAMA is underdense at $z < 0.1$ (Driver et al. 2011, which is above the median redshift of the faintest sample), a far more likely explanation is sample variance unaccounted for by the jack-knife errors.

Except for the brightest sample, the r_0 values seem to roughly follow the expectations of passive evolution. Of course, however, one has to worry about the selection effects. Using the volume-limited samples alone only gives some weak evidence of redshift evolution in r_0 between the lowest and second lowest redshift slices.

The highest luminosity sample shows some evidence of not following the passive evolution model. The volume-limited sample in particular shows stronger than expected clustering from a passive evolution model. However, given the size of the uncertainties the measurements are only 1σ–2σ away from the passive evolution model. A lack of evolution, compared to that expected from passive evolution, would suggest fast bias evolution. This would be consistent with many other observations of more massive and brighter galaxies showing little evolution in clustering with redshift (e.g. White et al. 2007; Brown et al. 2008; Coil et al. 2008; Meneux et al. 2008).

Moving back to our focus of model comparisons, the models show little dependence on clustering amplitude and luminosity. Both models predict a similar trend of r_0 versus luminosity. This lack of luminosity dependence is also in agreement with the Zehavi et al. (2011) bias fitting formula, up to the brightest sample where the L14 model r_0 values falls below the fitting formula. The models both predict much smaller r_0 values than the data in the highest luminosity bin, the models, unlike the data, also show evidence of evolution in the clustering with redshift in this sample.

4.3.3 Summary of model comparisons for luminosity samples

The models do a reasonable job at reproducing the amplitude of clustering as a function of luminosity for the samples fainter than L_r^*, and the L14 model is a good fit to many of the fainter samples. However, the models fail to reproduce the amplitude of our brightest sample. This underprediction particularly affects small-scale clustering. Also, recall Kim et al. (2009) found the dependence on luminosity was not correct for the Bower et al. (2006) model. Note that semi-analytic models have been shown to have a dependence on clustering with luminosity, but this evolution only starts to become apparent at the highest luminosity probed here (see e.g. Norberg et al. 2001). Again, the disagreements are particularly large at small scales, suggesting the modelling of satellite galaxies needs to be improved in the models.

4.4 Colour dependent clustering

Fig. 14 shows the clustering of our samples of red and blue GAMA galaxies (in black). In all redshift intervals we probe, red galaxies are more clustered than blue galaxies. We also note that the red galaxy correlation functions have their strongest clustering, relative to the reference line, at scales less than around 2 h^{-1} Mpc. This can be interpreted as red galaxies predominantly being in larger haloes with more satellite galaxies. The blue galaxy samples also show a relative increase in clustering on very small scales ($<0.3\,h^{-1}$ Mpc), but note that their clustering is still weaker than the reference power law.

In each panel of Fig. 14, we indicate the absolute magnitude range enclosing the central 68 per cent of the data. From Fig. 14, we can draw the following natural conclusions. First, for a given redshift slice, red galaxies are typically brighter than blue ones. Additionally, the absolute magnitude range of the central 68-percentile reduces with redshift and gets brighter with redshift. Finally, at fixed redshift, the change in clustering between red and blue galaxies is significantly larger than can be explained by any luminosity (or stellar mass) dependence of clustering alone. The models also show red galaxy samples have a larger amplitude and steeper 2PCFs than blue galaxies. At low redshifts ($z < 0.24$), the L14 model agrees with the measurements whilst the G14 model has too much small-scale clustering. In contrast, the G14 model shows better agreement in the two high-redshift slices, whilst the L14 model now has too little small-scale clustering.

The blue mock galaxy samples all have too low an amplitude, particularly at small scales. The size of the χ^2 values can leave us in no doubt that neither model successfully reproduces the clustering of blue galaxies. As the small-scale measurements are particularly discrepant, it is possible that too few satellite galaxies are blue. As these samples are magnitude-limited, another possibility is the model predicts blue satellites that are too faint. The predictions for blue galaxies being incorrect may not be too surprising, when one considers that the models predict a clear sequence of blue galaxies not seen in the data (Fig. 2). The models also do not reproduce the increase in clustering relative to the power law seen at very small scales ($<0.3\,h^{-1}$ Mpc). This could relate to an increase in star formation rate for close pairs of galaxies. This possibility will be explored in a future paper using star formation rate selected samples of GAMA galaxies (Gunawardhana et al. in preparation).

5 DISCUSSION AND CONCLUSIONS

We have studied the projected 2PCF of galaxies in GAMA. To do this, we used a modified version of the Cole (2011) approach to generate random catalogues; this method resulted in a set of random points with all of the properties of the real galaxies. The Cole (2011) approach allows sample selection cuts to be applied to both the data and the random catalogue, allowing the measurement of galaxy clustering as a function of diverse galaxy properties. Our modification, the inclusion of a window to limit the difference between the initial and cloned redshift, has the potential to limit the effects of galaxy evolution on random catalogues. This method should be followed up in later work, to test how effective it is on a wider selection of galaxy samples (e.g. not just selected on optical photometry) and to optimize the size of window used.

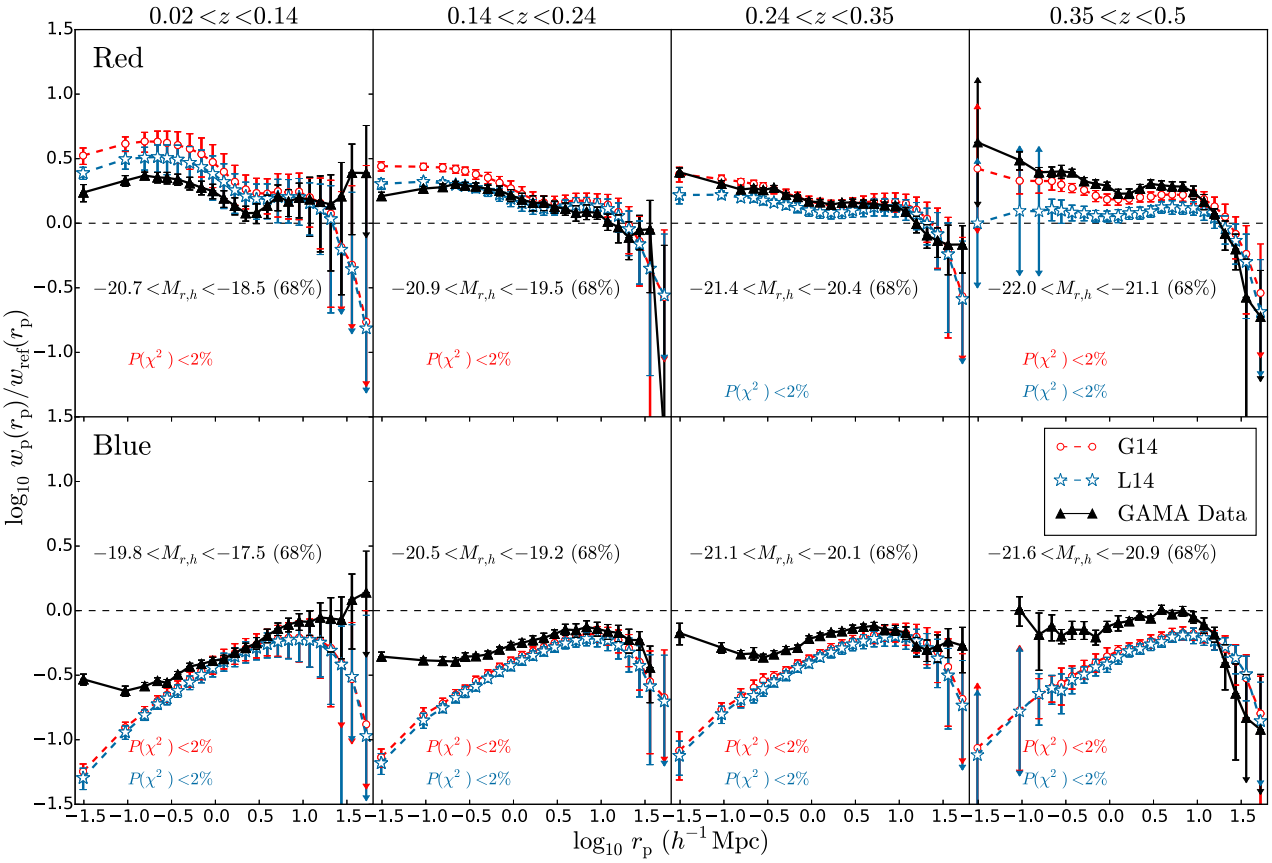

Figure 14. The projected correlation function of red galaxies (top) and blue galaxies (bottom) in different redshift slices. Also shown is the clustering of mock galaxies for the L14 model (blue) and the G14 model (red). The results have been divided by the reference power law defined in Section 3.2. Marked with $P <$ 2 per cent are samples for which the hypothesis that the data is a realization of the model has less than a 2 per cent probability, colour coded according to the model.

We compared volume-limited samples from SDSS of Zehavi et al. (2011) to volume-limited samples in GAMA, both with the redshift cuts of SDSS and with redshift cuts appropriate for the deeper, GAMA magnitude limit. We find good agreement with SDSS for our samples using the SDSS redshift limits. In our $-23.0 < M^{0.1}_{r,h} < -22.0$ sample and in our faintest sample, $-19.0 < M^{0.1}_{r,h} < -18.0$, both with the GAMA redshift limits, we find some disagreement between SDSS and GAMA. Given the expected uncertainties in our jack-knife covariance matrices, this could indicate the errors were underestimated. Our faintest sample, $-19.0 < M^{0.1}_{r,h} < -18.0$, shows less clustering than the SDSS data. Particularly relevant for this sample is the Driver et al. (2011) observation that GAMA is underdense at $z < 0.1$, which would indeed lead to lower clustering.

We have observed that more luminous, more massive and redder galaxies are more strongly clustered, in redshift slices between $z = 0$ and 0.5. Though in the two highest redshift slices, the GAMA selection function complicates the interpretation of this trend. More massive and luminous galaxies being more clustered is in agreement with previous measurements that show these trends exist at lower and higher redshift ranges (e.g. Zehavi et al. 2011; Christodoulou et al. 2012; Li et al. 2012; de la Torre et al. 2013; Marulli et al. 2013; Guo et al. 2014), and in a broad redshift bin encompassing all of our slices (Skibba et al. 2014). We also find that red galaxies have steeper correlation functions than blue galaxies in these redshift slices, again in agreement with clustering measured at higher (e.g. Coil et al. 2008; Guo et al. 2014) and lower (e.g. Zehavi et al. 2011) redshifts.

We fit power laws to our measurements and see an evolution in the apparent clustering strength of galaxies with redshift for samples less massive than $10^{10.5}\mathrm{M}_{\odot}h^{-2}$. We also evidence of this occurring for galaxies less luminous than around L_*. The evolution is in the direction of higher redshift galaxies being less clustered. Note however, many of our samples are not volume-limited and so will be affected by selection effects that are very likely to mimic this evolution. The volume-limited samples alone do show some evidence of higher redshift samples of the same luminosity or mass being less clustered, but this evidence is rather weak considering the size of the uncertainties.

In our most luminous sample ($\sim 3L_*$), which is volume-limited in three of the redshift slices, we see little evolution in clustering amplitude between samples with median redshifts of $z \sim 0.1$ and $z \sim 0.4$. Given our uncertainties, there is some weak evidence that this is less evolution than that expected from a simple, passive evolution model.

A lack of evolution in the clustering amplitude of brighter and more massive galaxies has been observed by other authors, and taken as evidence of a fast evolution of the bias of these objects (White et al. 2007; Brown et al. 2008; Meneux et al. 2008, 2009). This fast bias evolution has been connected to the merging and disruption of satellites (White et al. 2007; Brown et al. 2008).

Whilst the interpretation of these measurements is complicated by selection effects in the magnitude-limited samples, the strength and focus of this work is model comparisons. We use a model that utilizes a lightcone, and assign k-corrections to the model galaxies

in such a way to mimic the selections function of the survey. We find that the L14 and G14 semi-analytic models successfully predict the trends of clustering as a function of stellar mass. Both models have similar predictions for this trend, suggesting it is insensitive to differences in the adopted physics. In detail, there are places where the models disagree with the data, often in the regime of the one-halo term, which is too strong. Campbell et al. (2015) notes that estimating model masses from the colours, rather than taking them from the model, helps alleviate this problem for the L14 model.

We find the increase of clustering seen between our samples $-21.0 < M_{r,h} < -20.0$ and $-22.0 < M_{r,h} < -21.0$ is not reproduced by the models. This discrepancy is present in both models, but is a bigger problem for the L14 model. For the highest luminosity sample ($\sim 3L_r^*$), the models also predict too little small-scale clustering. The clustering of fainter galaxies is better modelled in the data, with the L14 model being particularly successful at reproducing the clustering of the $M_{r,h} > -20$ galaxy samples.

We have also shown that the trends of redshift evolution with mass and luminosity are qualitatively reproduced by the models (Figs 10 and 13), in that the more massive and more luminous samples show less redshift evolution. The redshift trends are most likely successfully reproduced thanks to the modelling of the GAMA apparent magnitude limit, showing the importance of applying observational effects when comparing galaxy formation models to data.

The clustering of red galaxies on large scales is successfully reproduced by the models. At $z > 0.35$, the L14 model underpredicts the clustering on small scales and at $z < 0.35$ the G14 model overpredicts clustering on small scales. Both models underpredict the clustering of blue galaxies, particularly on scales less than a few Mpc. The colour–magnitude diagram of the models is also very different to that of the data, the models have a much more clearly bimodal colour distribution.

These models give different predictions from one another for samples defined by mass, photometric properties and colour. This highlights the importance of testing the clustering of models using a variety of properties for sample selection, or, as Campbell et al. (2015) suggests, inferring the mass of the model galaxies from their photometric properties.

The models struggle to reproduce the clustering at small scales. Therefore, a suggested route to improvement is modifying the physics affecting satellite galaxies. Several authors have experimented with adding processes which remove satellite galaxies, or modify their luminosity or colour (e.g Font et al. 2008; Kim et al. 2009; Contreras et al. 2013). Kim et al. (2009) additionally found that processes affecting satellite galaxies can also change the dependence of clustering on luminosity. Modifying the satellite galaxy physics could also have an impact of the colour distribution and improve the clustering predictions of blue galaxies. Indeed, Font et al. (2008) found bluer satellites when applying a more realistic model of the stripping of gas from infalling satellite galaxies. Modifications to the satellite galaxy physics could also affect the overabundance of faint red galaxies in the models noted by McNaught-Roberts et al. (2014), or the excess of high-multiplicity groups of galaxies observed by Robotham et al. (2011). Finally, changing the colours of satellite galaxies can have knock-on effects for magnitude-limited samples, as model galaxies with red SEDs are *k*-corrected out of these samples at lower redshifts than blue galaxies. Such modifications should also be tested to see if they reproduce the lack of redshift evolution in the brightest samples where the physics affecting satellites galaxies is expected to play a role (White et al. 2007; Brown et al. 2008).

In conclusion, the G14 and L14 models reproduce the trends of clustering with mass and successfully predict the amplitude of clustering for galaxies fainter than L_r^*. They do, however, need improvement at small scales – in particular blue galaxies need stronger small-scale clustering. They also need to be improved in order to reproduce the clustering of galaxies slightly brighter than L_r^*, i.e. for our samples with median *r*-band magnitudes around $M_{r,h} \sim 21.3$. When these measurements are compared to models one must be careful to account for the selection effects in the magnitude-limited samples, for a realistic mock catalogue this could be as simple as applying an $r < 19.8$ apparent magnitude cut. An alternative is to choose the samples which are volume-limited. Indeed, in a future GAMA paper we intend to use the methodology here to produce volume-limited magnitude and mass threshold selected samples and carry out an HOD analysis on them (Palamara in preparation). In order to facilitate further model tests against these measurements, our results will be made available online at publication.[4]

ACKNOWLEDGEMENTS

DJF thanks Ariel Sanchez for useful discussions. The authors thank the anonymous referee for their useful comments. The authors also thank John Helly for his work on the VirgoDB. PN acknowledges the support of the Royal Society through the award of a University Research Fellowship and the European Research Council through receipt of a Starting Grant (DEGAS- 259586). MJIB acknowledges financial support from the Australian Research Council (FT100100280). JL acknowledges support from the Science and Technology Facilities Council (grant number ST/I000976/1). This work was supported by the Science and Technology Facilities Council [ST/L00075/1]. Data used in this paper will be available through the GAMA DB (http://www.gama-survey.org/) once the associated redshifts are publicly released.

GAMA is a joint European-Australian project based around a spectroscopic campaign using the Anglo-Australian Telescope. The GAMA input catalogue is based on data taken from the Sloan Digital Sky Survey and the UKIRT Infrared Deep Sky Survey. Complementary imaging of the GAMA regions is being obtained by a number of independent survey programmes including *GALEX* MIS, VST KIDS, VISTA VIKING, WISE, Herschel-ATLAS, GMRT and ASKAP providing UV to radio coverage. GAMA is funded by the STFC (UK), the ARC (Australia), the AAO, and the participating institutions. The GAMA website is http://www.gama-survey.org/.

This work used the DiRAC Data Centric system at Durham University, operated by the Institute for Computational Cosmology on behalf of the STFC DiRAC HPC Facility (www.dirac.ac.uk). This equipment was funded by BIS National E-infrastructure capital grant ST/K00042X/1, STFC capital grant ST/H008519/1, and STFC DiRAC Operations grant ST/K003267/1 and Durham University. DiRAC is part of the National E-Infrastructure.

REFERENCES

Abazajian K. N. et al., 2009, ApJS, 182, 543
Baldry I. K. et al., 2010, MNRAS, 404, 86
Baldry I. K. et al., 2012, MNRAS, 421, 621
Baldry I. K. et al., 2014, MNRAS, 441, 2440
Baugh C. M., Lacey C. G., Frenk C. S., Granato G. L., Silva L., Bressan A., Benson A. J., Cole S., 2005, MNRAS, 356, 1191
Bell E. F., McIntosh D. H., Katz N., Weinberg M. D., 2003, ApJS, 149, 289
Berlind A. A. et al., 2003, ApJ, 593, 1
Blake C. et al., 2013, MNRAS, 436, 3089
Blanton M. R., Roweis S., 2007, AJ, 133, 734
Blitz L., Rosolowsky E., 2006, ApJ, 650, 933

[4] http://icc.dur.ac.uk/data/

Bower R. G., Benson A. J., Malbon R., Helly J. C., Frenk C. S., Baugh C. M., Cole S., Lacey C. G., 2006, MNRAS, 370, 645
Brown M. J. I. et al., 2008, ApJ, 682, 937
Bruzual A. G., Charlot S., 1993, ApJ, 405, 538
Campbell D. J. R. et al., 2015, MNRAS, 452, 852
Carroll S. M., Press W. H., Turner E. L., 1992, ARA&A, 30, 499
Christodoulou L. et al., 2012, MNRAS, 425, 1527
Coil A. L. et al., 2008, ApJ, 672, 153
Coil A. L. et al., 2011, ApJ, 741, 8
Cole S., 2011, MNRAS, 416, 739
Cole S., Aragon-Salamanca A., Frenk C. S., Navarro J. F., Zepf S. E., 1994, MNRAS, 271, 781
Cole S., Lacey C. G., Baugh C. M., Frenk C. S., 2000, MNRAS, 319, 168
Colless M. et al., 2001, MNRAS, 328, 1039
Contreras S., Baugh C. M., Norberg P., Padilla N., 2013, MNRAS, 432, 2717
Cool R. J. et al., 2013, ApJ, 767, 118
de la Torre S. et al., 2013, A&A, 557, A54
Driver S. P. et al., 2011, MNRAS, 413, 971
Farrow D., 2013, PhD thesis, Durham University
Font A. S. et al., 2008, MNRAS, 389, 1619
Fry J. N., 1996, ApJ, 461, L65
Gaztañaga E., Scoccimarro R., 2005, MNRAS, 361, 824
Gonzalez-Perez V., Lacey C. G., Baugh C. M., Lagos C. D. P., Helly J., Campbell D. J. R., Mitchell P. D., 2014, MNRAS, 439, 264 (G14)
Guo H. et al., 2014, MNRAS, 441, 2398
Hamilton A. J. S., 1993, ApJ, 417, 19
Hill D. T. et al., 2011, MNRAS, 412, 765
Jackson J. C., 1972, MNRAS, 156, 1p
Jiang C. Y., Jing Y. P., Faltenbacher A., Lin W. P., Li C., 2008, ApJ, 675, 1095
Jiang C. Y., Jing Y. P., Han J., 2014, ApJ, 790, 7
Kaiser N., 1987, MNRAS, 227, 1
Kauffmann G., White S. D. M., Guiderdoni B., 1993, MNRAS, 264, 201
Kennicutt R. C., Jr, 1983, ApJ, 272, 54
Kim H.-S., Baugh C. M., Cole S., Frenk C. S., Benson A. J., 2009, MNRAS, 400, 1527
Komatsu E. et al., 2011, ApJS, 192, 18
Lacey C., Cole S., 1993, MNRAS, 262, 627
Lagos C. D. P., Lacey C. G., Baugh C. M., Bower R. G., Benson A. J., 2011, MNRAS, 416, 1566
Lagos C. d. P., Bayet E., Baugh C. M., Lacey C. G., Bell T. A., Fanidakis N., Geach J. E., 2012, MNRAS, 426, 2142
Lemson G., the Virgo Consortium, 2006, preprint (astro-ph/0608019)
Li C., Kauffmann G., Jing Y. P., White S. D. M., Börner G., Cheng F. Z., 2006, MNRAS, 368, 21
Li C. et al., 2012, MNRAS, 419, 1557
Lin H., Yee H. K. C., Carlberg R. G., Morris S. L., Sawicki M., Patton D. R., Wirth G., Shepherd C. W., 1999, ApJ, 518, 533
Liske J. et al., 2015, MNRAS, submitted
Loveday J. et al., 2012, MNRAS, 420, 1239
Loveday J. et al., 2015, MNRAS, 451, 1540
McCracken H. J., Ilbert O., Mellier Y., Bertin E., Guzzo L., Arnouts S., Le Fèvre O., Zamorani G., 2008, A&A, 479, 321
McCracken H. J. et al., 2015, MNRAS, 449, 901
McNaught-Roberts T. et al., 2014, MNRAS, 445, 2125
Maraston C., 2005, MNRAS, 362, 799
Marín F. A. et al., 2013, MNRAS, 432, 2654
Marulli F. et al., 2013, A&A, 557, A17
Meneux B. et al., 2008, A&A, 478, 299
Meneux B. et al., 2009, A&A, 505, 463
Merson A. I. et al., 2013, MNRAS, 429, 556
Mitchell P. D., Lacey C. G., Baugh C. M., Cole S., 2013, MNRAS, 435, 87
Norberg P. et al., 2001, MNRAS, 328, 64
Norberg P. et al., 2002, MNRAS, 332, 827
Norberg P., Baugh C. M., Gaztañaga E., Croton D. J., 2009, MNRAS, 396, 19
Petrosian V., 1976, ApJ, 209, L1
Phleps S., Peacock J. A., Meisenheimer K., Wolf C., 2006, A&A, 457, 145
Pollo A. et al., 2006, A&A, 451, 409
Robotham A. et al., 2010, PASA, 27, 76
Robotham A. S. G. et al., 2011, MNRAS, 416, 2640
Skibba R. A. et al., 2014, ApJ, 784, 128
Springel V. et al., 2005, Nature, 435, 629
Strauss M. A. et al., 2002, AJ, 124, 1810
Taylor E. N. et al., 2011, MNRAS, 418, 1587
Tonry J. L., Blakeslee J. P., Ajhar E. A., Dressler A., 2000, ApJ, 530, 625
Tormen G., 1997, MNRAS, 290, 411
White S. D. M., Frenk C. S., 1991, ApJ, 379, 52
White S. D. M., Rees M. J., 1978, MNRAS, 183, 341
White M., Zheng Z., Brown M. J. I., Dey A., Jannuzi B. T., 2007, ApJ, 655, L69
York D. G. et al., 2000, AJ, 120, 1579
Zehavi I. et al., 2002, ApJ, 571, 172
Zehavi I. et al., 2005, ApJ, 630, 1
Zehavi I. et al., 2011, ApJ, 736, 59
Zheng Z. et al., 2005, ApJ, 633, 791

APPENDIX A: THE EFFECT OF P, Q AND WINDOWED RANDOMS ON THE CORRELATION FUNCTION

In this paper, we utilize a random catalogue generated using a new, windowed approach. We also use a different combination of the luminosity function evolution parameters $Q = 1.45$, $P = 0.0$ to a different set of parameters taken from an earlier draft of Loveday et al. (2015): $Q = 0.81, P = 1.45$. To test for any biases introduced by this, we compare results of using three different random catalogues: the randoms used in our measurements, the same P and Q as our

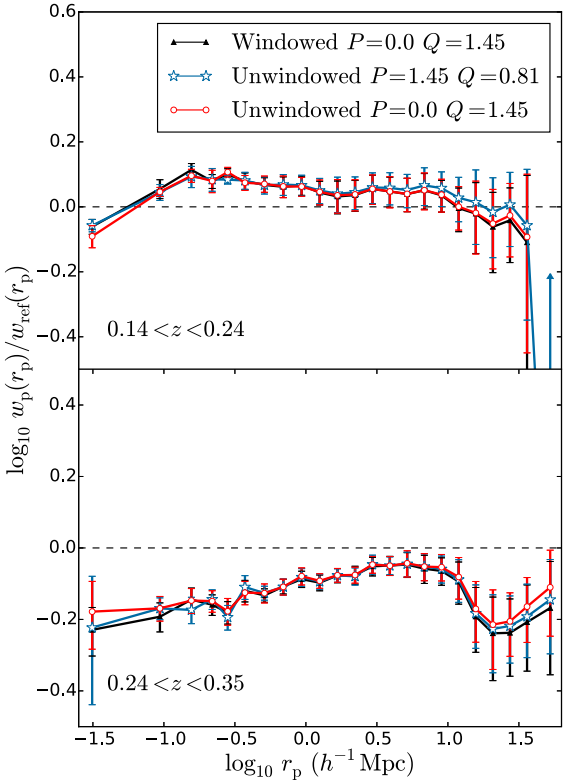

Figure A1. The projected 2PCF of $10.00 < \log_{10} M_*/\mathrm{M}_\odot\, h^{-2} < 10.50$ galaxies in two different redshift slices, as indicated. The different lines represent different methods of generating a random catalogue with which to measure clustering, each is labelled in the legend. It can be seen that the our choice of random catalogue does not have a significant effect on our measurements.

random catalogue but without the window function and a different P and Q with and without the window function. For this purpose, we use a mass selected sample, as this avoids changes in the sample definition arising due to a different value of Q. We choose the $10.00 < \log_{10} M_*/\mathrm{M}_\odot\, h^{-2} < 10.50$ mass bin, and use the redshift ranges $0.14 < z < 0.24$ and $0.24 < z < 0.35$. These redshift slices encompass a large underdensity in the $n(z)$, where one might expect to see the largest differences between the random catalogues.

In Fig. A1, we show the results. The most difference appears at large scales; with the measurements using the windowed catalogue showing a lower clustering amplitude than the results from the two random catalogues without windowing. The two unwindowed results also show some deviation on large scales. Note, however, that the differences are much smaller than the error bars for both of the samples, so much so that the conclusions of this paper will not be affected.

APPENDIX B: POWER-LAW FIT TABLES AND MOCK SAMPLE PROPERTIES

In Table B1, we show the results from our power-law fits to our samples of GAMA galaxies. Uncertainties are given in brackets, and were derived from fitting power laws to each jack-knife realization separately. Also given are the r_0 values found from fixing the slope of the power law, γ, rather than allow it to vary freely. The difference in the recovered r_0 values is small.

Tables B2 and B3 give the sample properties, and standard deviations (in brackets) of one realization of the G14 and L14 models, respectively. The magnitudes have been adjusted in order to match their luminosity functions to the real GAMA data (see Section 2.3.3), as such the sample sizes are much more similar to the real data for luminosity-defined samples than mass- or colour-defined samples.

Table B1. The recovered values from power-law fits to the clustering, $r_{0,\gamma\ \mathrm{fixed}}$ are the results of fitting the data with a fixed value of $\gamma = 1.8$. Jack-knife errors are given in brackets. We see red galaxies have steeper 2PCFs, and that the amplitude of the 2PCF increases with magnitude and mass, regardless as to whether γ is also fit or not. Samples marked with asterisks are magnitude limited, so should be treated with careful consideration of the GAMA selection function. Samples without asterisks are volume-limited, and can be treated at face value.

Sample	z_{min}	z_{max}	r_0	γ	$r_{0,\gamma\ \mathrm{fixed}}$
$-18.00 < M_{r,h} < -17.00$	0.02	0.14*	3.68 (0.31)	1.81 (0.09)	3.69 (0.27)
$-19.00 < M_{r,h} < -18.00$	0.02	0.14*	4.57 (0.37)	1.74 (0.06)	4.44 (0.26)
	0.14	0.24*	4.51 (0.69)	1.84 (0.05)	4.52 (0.70)
$-20.00 < M_{r,h} < -19.00$	0.02	0.14	5.35 (0.51)	1.70 (0.07)	5.07 (0.36)
	0.14	0.24*	4.91 (0.22)	1.78 (0.03)	4.86 (0.17)
	0.24	0.35*	4.05 (0.17)	1.69 (0.05)	4.09 (0.18)
$-21.00 < M_{r,h} < -20.00$	0.02	0.14	5.58 (0.75)	1.76 (0.07)	5.45 (0.53)
	0.14	0.24	5.39 (0.28)	1.78 (0.04)	5.33 (0.19)
	0.24	0.35*	5.04 (0.09)	1.76 (0.02)	4.98 (0.07)
	0.35	0.50*	4.82 (0.27)	1.62 (0.06)	4.84 (0.26)
$-22.00 < M_{r,h} < -21.00$	0.02	0.14	6.59 (0.58)	1.77 (0.08)	6.49 (0.44)
	0.14	0.24	6.12 (0.32)	1.87 (0.05)	6.30 (0.25)
	0.24	0.35	6.47 (0.18)	1.79 (0.02)	6.45 (0.16)
	0.35	0.50*	6.38 (0.25)	1.81 (0.03)	6.40 (0.20)
$-23.00 < M^{0.1}_{r,h} < -22.00$	0.01	0.50	9.39 (0.50)	1.99 (0.10)	9.56 (0.44)
$-22.00 < M^{0.1}_{r,h} < -21.00$	0.01	0.38	6.65 (0.10)	1.77 (0.01)	6.60 (0.09)
$-21.00 < M^{0.1}_{r,h} < -20.00$	0.01	0.26	5.72 (0.28)	1.75 (0.03)	5.55 (0.20)
$-20.00 < M^{0.1}_{r,h} < -19.00$	0.01	0.18	5.27 (0.42)	1.74 (0.04)	5.08 (0.31)
$-19.00 < M^{0.1}_{r,h} < -18.00$	0.01	0.12	3.97 (0.33)	1.87 (0.06)	4.09 (0.27)
$8.50 < \log_{10} M_*/\mathrm{M}_\odot\, h^{-2} < 9.50$	0.02	0.05	3.28 (0.42)	2.24 (0.21)	4.86 (0.38)
	0.02	0.14*	4.00 (0.22)	1.73 (0.05)	3.95 (0.21)
	0.14	0.24*	3.70 (0.19)	1.66 (0.03)	3.65 (0.17)
$9.50 < \log_{10} M_*/\mathrm{M}_\odot\, h^{-2} < 10.00$	0.02	0.14	5.84 (0.64)	1.77 (0.07)	5.72 (0.37)
	0.14	0.24*	4.81 (0.24)	1.77 (0.03)	4.75 (0.20)
	0.24	0.35*	3.44 (0.11)	1.64 (0.05)	3.64 (0.09)
$10.00 < \log_{10} M_*/\mathrm{M}_\odot\, h^{-2} < 10.50$	0.02	0.14	5.93 (0.71)	1.82 (0.07)	6.01 (0.54)
	0.14	0.18	5.94 (0.46)	1.86 (0.05)	6.35 (0.36)
	0.14	0.24*	5.67 (0.27)	1.85 (0.04)	5.86 (0.17)
	0.24	0.35*	4.81 (0.13)	1.73 (0.02)	4.71 (0.11)
	0.35	0.50*	4.49 (0.20)	1.69 (0.04)	4.65 (0.19)
$10.50 < \log_{10} M_*/\mathrm{M}_\odot\, h^{-2} < 11.00$	0.02	0.14	6.84 (0.62)	1.75 (0.09)	6.69 (0.47)
	0.14	0.24	6.37 (0.34)	1.93 (0.04)	6.78 (0.30)
	0.24	0.29	5.76 (0.28)	1.93 (0.03)	6.65 (0.24)
	0.24	0.35*	6.37 (0.20)	1.84 (0.02)	6.50 (0.17)
	0.35	0.50*	6.15 (0.22)	1.78 (0.03)	6.10 (0.16)
$11.00 < \log_{10} M_*/\mathrm{M}_\odot\, h^{-2} < 11.50$	0.24	0.35	8.42 (0.37)	1.76 (0.03)	8.33 (0.34)
	0.35	0.37	8.06 (1.33)	2.14 (0.11)	10.88 (1.19)
	0.35	0.50*	8.17 (0.47)	1.88 (0.05)	8.38 (0.44)

Table B1 *– continued.*

Sample	$z_{\rm min}$	$z_{\rm max}$	r_0	γ	$r_{0,\gamma\ \rm fixed}$
Red	0.02	0.14*	6.25 (0.53)	2.03 (0.07)	7.13 (0.45)
	0.14	0.24*	6.37 (0.31)	1.96 (0.03)	7.04 (0.25)
	0.24	0.35*	6.49 (0.15)	1.90 (0.01)	6.79 (0.14)
	0.35	0.50*	7.50 (0.29)	1.89 (0.02)	7.82 (0.25)
Blue	0.02	0.14*	3.34 (0.14)	1.52 (0.02)	3.03 (0.10)
	0.14	0.24*	3.89 (0.14)	1.63 (0.03)	3.63 (0.10)
	0.24	0.35*	4.09 (0.11)	1.64 (0.02)	4.00 (0.10)
	0.35	0.50*	4.80 (0.10)	1.69 (0.03)	4.85 (0.10)

Table B2. Different mock galaxy samples, sample sizes and median properties for one G14 model realization of GAMA. The subscript 'med' indicates the values are medians. Where maximum redshift has an asterisk, the sample is not volume limited. In samples without an asterisk at least 95 per cent of the members are volume limited. Values in brackets are rms scatter.

Sample	$z_{\rm min}$	$z_{\rm max}$	$N_{\rm gals}$	$z_{\rm med}$	$M_{\rm med}$	$\log_{10}(M_*/{\rm M}_\odot\, h^{-2})_{\rm med}$	$(g-r)_{0,\rm med}$
$-18.00 < M_{r,h} < -17.00$	0.02	0.07	2965	0.05	−17.46 (0.28)	8.83 (0.26)	0.29 (0.17)
	0.02	0.14*	5907	0.07	−17.59 (0.27)	8.83 (0.25)	0.27 (0.17)
$-19.00 < M_{r,h} < -18.00$	0.02	0.11	7402	0.08	−18.48 (0.29)	9.20 (0.30)	0.30 (0.18)
	0.02	0.14*	12979	0.10	−18.55 (0.27)	9.21 (0.30)	0.29 (0.18)
	0.14	0.24*	2894	0.15	−18.85 (0.12)	9.28 (0.33)	0.30 (0.19)
$-20.00 < M_{r,h} < -19.00$	0.02	0.14	11689	0.11	−19.47 (0.29)	9.71 (0.37)	0.43 (0.20)
	0.14	0.17	7029	0.15	−19.45 (0.28)	9.75 (0.39)	0.51 (0.20)
	0.14	0.24*	26387	0.19	−19.61 (0.27)	9.78 (0.39)	0.49 (0.21)
	0.24	0.35*	2343	0.25	−19.91 (0.09)	9.65 (0.29)	0.27 (0.17)
$-21.00 < M_{r,h} < -20.00$	0.02	0.14	6968	0.11	−20.40 (0.28)	10.26 (0.36)	0.61 (0.21)
	0.14	0.24	22285	0.20	−20.39 (0.28)	10.28 (0.35)	0.61 (0.21)
	0.24	0.35*	35746	0.28	−20.56 (0.26)	10.24 (0.36)	0.50 (0.21)
	0.35	0.50*	3644	0.37	−20.87 (0.14)	10.05 (0.28)	0.27 (0.17)
$-22.00 < M_{r,h} < -21.00$	0.02	0.14	1835	0.11	−21.28 (0.25)	10.72 (0.32)	0.70 (0.20)
	0.14	0.24	5838	0.20	−21.28 (0.25)	10.73 (0.32)	0.70 (0.20)
	0.24	0.35	15354	0.30	−21.29 (0.25)	10.72 (0.32)	0.66 (0.20)
	0.35	0.37	3316	0.36	−21.29 (0.26)	10.72 (0.32)	0.64 (0.20)
	0.35	0.50*	17073	0.40	−21.41 (0.26)	10.64 (0.35)	0.48 (0.21)
$8.50 < M_* < 9.50$	0.02	0.05	3066	0.04	−17.49 (0.89)	8.92 (0.28)	0.43 (0.16)
	0.02	0.14*	20046	0.09	−18.34 (0.76)	9.11 (0.26)	0.27 (0.14)
	0.14	0.24*	7525	0.17	−19.23 (0.30)	9.37 (0.12)	0.25 (0.07)
$9.50 < M_* < 10.00$	0.02	0.14*	10713	0.11	−19.44 (0.63)	9.73 (0.14)	0.54 (0.16)
	0.14	0.24*	19616	0.19	−19.79 (0.47)	9.77 (0.14)	0.35 (0.15)
	0.24	0.35*	12697	0.28	−20.34 (0.28)	9.84 (0.12)	0.27 (0.08)
$10.00 < M_* < 10.50$	0.02	0.14	5746	0.11	−20.18 (0.58)	10.20 (0.14)	0.66 (0.15)
	0.14	0.18	5155	0.16	−20.14 (0.57)	10.20 (0.14)	0.66 (0.15)
	0.14	0.24*	18085	0.20	−20.17 (0.53)	10.22 (0.14)	0.65 (0.15)
	0.24	0.35*	19509	0.28	−20.72 (0.42)	10.25 (0.15)	0.44 (0.16)
	0.35	0.50*	8752	0.40	−21.23 (0.30)	10.24 (0.14)	0.29 (0.09)
$10.50 < M_* < 11.00$	0.02	0.14	3455	0.11	−20.71 (0.69)	10.73 (0.14)	0.76 (0.11)
	0.14	0.24*	11227	0.20	−20.69 (0.61)	10.71 (0.14)	0.75 (0.11)
	0.24	0.29*	8747	0.27	−20.83 (0.43)	10.71 (0.14)	0.72 (0.11)
	0.24	0.35*	18649	0.29	−20.94 (0.40)	10.72 (0.14)	0.71 (0.11)
	0.35	0.50*	7885	0.39	−21.39 (0.33)	10.80 (0.15)	0.67 (0.16)
$11.00 < M_* < 11.50$	0.24	0.35*	3114	0.30	−21.75 (0.50)	11.09 (0.09)	0.75 (0.05)
	0.35	0.37	609	0.36	−21.79 (0.32)	11.10 (0.09)	0.74 (0.05)
	0.35	0.50*	4377	0.41	−21.84 (0.28)	11.11 (0.09)	0.73 (0.05)
Red	0.02	0.14*	19247	0.10	−19.23 (1.37)	9.87 (0.65)	0.63 (0.10)
$(g-r)_0 + 0.03(M_{r,h} - M^*_{r,h}) > 0.498$	0.14	0.24*	31606	0.19	−20.07 (0.70)	10.35 (0.38)	0.69 (0.09)
	0.24	0.35*	28164	0.28	−20.80 (0.51)	10.67 (0.28)	0.71 (0.08)
	0.35	0.50*	10034	0.39	−21.53 (0.38)	10.97 (0.21)	0.72 (0.06)
Blue	0.02	0.14*	24008	0.09	−18.72 (1.27)	9.18 (0.53)	0.26 (0.07)
$(g-r)_0 + 0.03(M_{r,h} - M^*_{r,h}) < 0.498$	0.14	0.24*	26135	0.19	−19.88 (0.70)	9.68 (0.34)	0.30 (0.08)
	0.24	0.35*	26245	0.29	−20.63 (0.49)	10.01 (0.28)	0.30 (0.09)
	0.35	0.50*	12622	0.40	−21.25 (0.40)	10.26 (0.26)	0.29 (0.10)

Table B3. Different mock galaxy samples, sample sizes and median properties for one L14 model realization of GAMA. The subscript 'med' indicates the values are medians. Where maximum redshift has an asterisk, the sample is not volume-limited. In samples without an asterisk at least 95 per cent of the members are volume-limited. Values in brackets are rms scatter.

Sample	$z_{\rm min}$	$z_{\rm max}$	$N_{\rm gals}$	$z_{\rm med}$	$M_{\rm med}$	$\log_{10}(M_*/{\rm M}_\odot\, h^{-2})_{\rm med}$	$(g-r)_{0,{\rm med}}$
$-18.00 < M_{r,h} < -17.00$	0.02	0.07	2982	0.05	−17.46 (0.28)	8.82 (0.30)	0.41 (0.15)
	0.02	0.14*	5922	0.07	−17.59 (0.27)	8.82 (0.29)	0.39 (0.15)
$-19.00 < M_{r,h} < -18.00$	0.02	0.11	7348	0.08	−18.49 (0.29)	9.21 (0.31)	0.42 (0.15)
	0.02	0.14*	12815	0.10	−18.55 (0.27)	9.22 (0.31)	0.41 (0.15)
	0.14	0.24*	2887	0.15	−18.85 (0.12)	9.27 (0.30)	0.41 (0.16)
$-20.00 < M_{r,h} < -19.00$	0.02	0.14	11665	0.11	−19.47 (0.29)	9.65 (0.35)	0.51 (0.16)
	0.14	0.17	7242	0.15	−19.45 (0.29)	9.67 (0.37)	0.53 (0.17)
	0.14	0.24*	26443	0.19	−19.61 (0.27)	9.70 (0.38)	0.53 (0.17)
	0.24	0.35*	2560	0.25	−19.91 (0.09)	9.62 (0.26)	0.36 (0.15)
$-21.00 < M_{r,h} < -20.00$	0.02	0.14	6934	0.11	−20.41 (0.28)	10.18 (0.40)	0.62 (0.18)
	0.14	0.24	22310	0.20	−20.40 (0.28)	10.22 (0.40)	0.63 (0.18)
	0.24	0.35*	35739	0.28	−20.56 (0.27)	10.16 (0.41)	0.56 (0.19)
	0.35	0.50*	3563	0.37	−20.86 (0.15)	10.00 (0.31)	0.37 (0.16)
$-22.00 < M_{r,h} < -21.00$	0.02	0.14	1833	0.11	−21.28 (0.25)	10.63 (0.39)	0.65 (0.18)
	0.14	0.24	5843	0.20	−21.28 (0.25)	10.65 (0.38)	0.64 (0.18)
	0.24	0.35	15349	0.30	−21.28 (0.25)	10.63 (0.38)	0.61 (0.18)
	0.35	0.37	3399	0.36	−21.29 (0.26)	10.64 (0.38)	0.59 (0.17)
	0.35	0.50*	17320	0.40	−21.42 (0.26)	10.47 (0.39)	0.49 (0.18)
$8.50 < M_* < 9.50$	0.02	0.05*	3077	0.04	−17.46 (0.94)	8.92 (0.28)	0.55 (0.14)
	0.02	0.14*	19994	0.09	−18.36 (0.80)	9.12 (0.26)	0.38 (0.12)
	0.14	0.24*	9080	0.17	−19.29 (0.31)	9.36 (0.12)	0.36 (0.08)
$9.50 < M_* < 10.00$	0.02	0.14*	11290	0.11	−19.45 (0.71)	9.72 (0.14)	0.58 (0.13)
	0.14	0.24*	20525	0.19	−19.86 (0.50)	9.76 (0.14)	0.44 (0.12)
	0.24	0.35*	15610	0.28	−20.39 (0.31)	9.82 (0.12)	0.38 (0.09)
$10.00 < M_* < 10.50$	0.02	0.14	5550	0.11	−20.09 (0.66)	10.19 (0.14)	0.68 (0.11)
	0.14	0.18	5102	0.16	−20.06 (0.65)	10.20 (0.14)	0.68 (0.12)
	0.14	0.24*	16659	0.20	−20.14 (0.61)	10.21 (0.14)	0.67 (0.12)
	0.24	0.35*	18009	0.29	−20.82 (0.47)	10.22 (0.14)	0.53 (0.12)
	0.35	0.50*	9983	0.40	−21.33 (0.33)	10.22 (0.14)	0.42 (0.09)
$10.50 < M_* < 11.00$	0.02	0.14	2806	0.11	−20.71 (0.58)	10.71 (0.14)	0.78 (0.10)
	0.14	0.24*	9615	0.20	−20.66 (0.53)	10.72 (0.14)	0.78 (0.10)
	0.24	0.29*	7770	0.27	−20.76 (0.44)	10.72 (0.14)	0.76 (0.10)
	0.24	0.35*	16067	0.29	−20.88 (0.42)	10.75 (0.14)	0.75 (0.10)
	0.35	0.50*	6316	0.39	−21.47 (0.38)	10.78 (0.15)	0.62 (0.14)
$11.00 < M_* < 11.50$	0.24	0.35*	4280	0.30	−21.42 (0.51)	11.09 (0.09)	0.79 (0.07)
	0.35	0.37	760	0.36	−21.50 (0.35)	11.10 (0.09)	0.78 (0.06)
	0.35	0.50*	3912	0.40	−21.68 (0.35)	11.12 (0.10)	0.77 (0.08)
Red	0.02	0.14*	20986	0.10	−19.07 (1.38)	9.80 (0.65)	0.65 (0.09)
$(g-r)_0 + 0.03(M_{r,h} - M^*_{r,h}) > 0.548$	0.14	0.24*	31557	0.19	−20.06 (0.67)	10.29 (0.41)	0.70 (0.09)
	0.24	0.35*	27728	0.28	−20.77 (0.47)	10.68 (0.32)	0.73 (0.08)
	0.35	0.50*	7944	0.39	−21.46 (0.36)	10.98 (0.24)	0.75 (0.07)
Blue	0.02	0.14*	22218	0.10	−18.80 (1.30)	9.18 (0.53)	0.36 (0.07)
$(g-r)_0 + 0.03(M_{r,h} - M^*_{r,h}) < 0.548$	0.14	0.24*	26243	0.19	−19.88 (0.73)	9.62 (0.33)	0.39 (0.08)
	0.24	0.35*	26870	0.29	−20.65 (0.54)	9.95 (0.29)	0.40 (0.09)
	0.35	0.50*	14824	0.40	−21.34 (0.43)	10.22 (0.29)	0.41 (0.10)

This paper has been typeset from a TEX/LATEX file prepared by the author.